https://doi.org/10.5194/egusphere-2026-5245
Preprint. Discussion started: 28 September 2026

The Added Value of Amazon observations to estimate methane budget over South American river basins in a global inversion system

Shrutika Wagh[1,2], Luana S. Basso[1], Ayan S. Fleischmann[3], Joao Henrique Fernandes Amaral[4], John Melack[5], Jost Lavric[6], David Walter[7], Stijn Hantson[4], Julia Marshall[8,9], Chris Wilson[10,11], Youmi Oh[12,13] , Lori Bruhwiler[12], John B. Miller[12], Corinne Vigouroux[14], Christian Rödenbeck[1], and Santiago Botía[1]

Correspondence to: Shrutika Wagh (swagh@bgc-jena.mpg.de)

[1]Max Planck Institute for Biogeochemistry, Hans-Knoell-Straße 10, 07745 Jena, Germany
[2]Friedrich Schiller University Jena Institute of Geosciences, Burgweg 11, 07749 Jena, Germany
[3]Instituto de Desenvolvimento Sustentável Mamirauá, Tefé, Amazonas, Brasil
[4]School of Sciences and Engineering, Universidad del Rosario Bogotá, Colombia
[5]Earth Research Institute University of California Santa Barbara, Santa Barbara, USA
[6]Acoem GmbH, Hallbergmoos, Germany
[7]Max Planck Institute for Chemistry, Hahn-Meitner-Weg 1, D-55128 Mainz
[8]Deutsches Zentrum für Luft- und Raumfahrt, Institut für Physik der Atmosphäre, Oberpfaffenhofen, Germany
[9]Leipziger Institut für Meteorologie, Universität Leipzig, Leipzig, Germany
[10]National Centre for Earth Observation University of Leeds, Leeds, UK
[11] School of Earth and Environment, University of Leeds, Leeds, UK
[12]Global Monitoring Laboratory, National Oceanic and Atmospheric Administration, Boulder, CO, USA
[13]Cooperative Institute for Research in Environmental Science, University of Colorado, Boulder, CO, USA
[14]Royal Belgian Institute for Space Aeronomy (BIRA-IASB), Brussels, Belgium

https://doi.org/10.5194/egusphere-2026-5245
Preprint. Discussion started: 28 September 2026

Abstract:

Tropical South America is one of the world's largest natural methane (CH_4) emitting regions, yet regional methane budgets remain highly uncertain due to poorly constrained wetland emissions and sparse atmospheric observations. Here, we quantify methane emissions from the Amazon, Orinoco, and Paraná river basins for 2010–2019 using the Jena CarboScope atmospheric inverse modelling system. We investigate the variability in methane budget through a series of sensitivity. Our inversion estimates methane emissions of 4.44 ± 0.88 Tg CH_4 yr^{-1} for the Orinoco, 28.60 ± 5.15 Tg CH_4 yr^{-1} for the Amazon, and 30.10 ± 3.95 Tg CH_4 yr^{-1} for the Paraná basin, together accounting for ~59% of the total estimated South American methane emissions (105.5 ± 11.10 Tg CH_4 yr^{-1}). The inversion substantially modifies the seasonality and interannual variability of prior wetland emissions in all three basins. The dominant source of posterior variability differs among basins. The data-sparse Orinoco is most sensitive to the wetland prior, indicating strong dependence on prior information. Regional observations mainly constrain the Amazon, which accounts for 55% of the variability in South American posterior methane emissions. The Paraná is largely insensitive to regional observations and is constrained primarily by the global network. These results show that uncertainty sources vary across tropical South America. Improving wetland priors and expanding regional atmospheric measurements are essential for reducing uncertainty in regional methane budgets.

https://doi.org/10.5194/egusphere-2026-5245
Preprint. Discussion started: 28 September 2026

1. Introduction

Following a temporary pause in the early 2000s, atmospheric methane (CH_4) has risen at a higher variable rate since 2007 (Thoning et al., 2022). The cause of this renewed growth is still under debate (Nisbet et al., 2019, 2023; Turner et al., 2019). Several mechanisms have been suggested and progressively refined (Nisbet et al., 2016; Rigby et al., 2017; Saunois et al., 2017; Turner et al., 2017; Jackson et al., 2020, 2024), with a positive contribution from microbial and fossil sources as the most consistently supported explanations (Schwietzke et al., 2016; Nisbet et al., 2019, 2023; Jackson et al., 2020; Basu et al., 2022). Furthermore, the rising emissions have been each time more attributed to tropical wetlands areas (Saunois et al., 2017; Jackson et al., 2020; Wilson et al., 2021, Basu et al., 2022, Drinkwater et al., 2023; Oh et al., 2026), known to be large natural methane sources. However, large uncertainties remain in estimates of total methane emissions for regions such as South America, Africa, and India, with estimates differing by 40–60% among available inventories and inversion systems (Saunois et al., 2025).

Across the pantropics, South America is one of largest contributors of methane emissions from wetlands (~13% of the total global wetland emission) (Kirschke et al., 2013; Saunois et al., 2025), but there is a large discrepancy among process-based models (bottom-up approach), with an estimated range larger than that of atmospheric transport inversions (top-down approach) (Saunois et al., 2025). In the recent Global Methane Budget (Saunois et al., 2025), it was shown that the category of "combined wetland and inland freshwater emissions" dominates the contribution to regional emissions in South America for 2010-2019, with ranges based on top-down estimates going from 20–33 Tg CH_4 yr^{-1} in Brazil, to 14–33 Tg CH_4 yr^{-1} in southwestern South America, and 6–10 Tg CH_4 yr^{-1} in northern South America, corresponding to approximately 52%, 58%, and 50% of total regional methane emissions in Brazil, southwestern South America, and northern South America, respectively. Unlike most regions of the world, where direct anthropogenic emissions account for more than half of total methane emissions, South America is characterized by the substantial contribution of natural wetland and inland freshwater sources. Consequently, uncertainties in wetland and inland freshwater extent and emissions, which dominate the regional methane budget, are the dominant source of uncertainty and request a better constraint of these fluxes from a top-down perspective.

https://doi.org/10.5194/egusphere-2026-5245
Preprint. Discussion started: 28 September 2026

The Amazon, the Orinoco, and the Parana basins (Fig. 1) are the largest river basins in South America, and the most relevant ones for natural methane emissions, given their large wetlands and inland freshwater systems. Several studies have focused on methane emissions from the Amazon river basin. For example, Wilson et al. (2016, 2021) used GOSAT satellite retrievals and the TOMCAT/INVICAT inversion system to identify large and increasing emissions from eastern Amazonia. Basso et al. (2021) used regular aircraft vertical profiles over several Amazonian sites to derive regional flux estimates that amounted to 46.2 ± 10.3 Tg CH_4 yr^{-1}, attributing large emissions to the eastern part of the basin, consistent with previous studies (Miller et al., 2007; Basso et al., 2016; Wilson et al., 2021). Similarly, Neves et al. (2026) uses the aircraft vertical profile data over Amazon and estimates 40-50 Tg CH_4 yr^{-1}. Tunnicliffe et al. (2020) used a regional inversion to revise Brazilian emissions downward relative to previous estimates (i.e. Janardanan et al., 2020) for a total budget of 33.6 ± 3.6 Tg CH_4 yr^{-1}, with wetlands contributing 13.0 ± 1.9 Tg CH_4 yr^{-1}, substantially below estimates from several global inversions. More recently, Hancock et al. (2025) used a high-resolution analytical inversion using both TROPOMI and GOSAT satellite retrievals to quantify national emissions across South America, finding posterior wetland fluxes relatively consistent with WetCHARTs wetland emission model (Bloom et al., 2017) prior inventories for the Amazon. Field data collection on both tree trunks and water diffusive and ebullitive fluxes has been conducted over the past decades. These observations have also been regionalized to derive basin-scale bottom-up methane budgets, although substantial uncertainties remain due to the challenges of scaling sparse field measurements across the heterogeneous Amazon landscape and the overall budget is still uncertain (Melack et al., 2004; Pangala et al., 2017; Barbosa et al., 2020; Melack et al., 2022). Despite the large number of studies conducted over the past decade, no clear consensus has emerged regarding the total methane budget of the Amazon basin, let alone its interannual variability, and there remains several challenges in methane regionalization across the basin (Melack et al., 2022). These persistent discrepancies highlight the need for further studies to better constrain methane emissions from tropical South America.

In contrast, the other two basins (Orinoco and Paraná) remain relatively understudied in terms of anthropogenic and natural methane emissions. The Orinoco Basin is seasonally flooded, with seasonally flooded savannas representing the dominant methane source (Amaral et al., 2026) with emission estimates ranges from 3.27 - 5.31 Tg CH_4 yr^{-1}. The Paraná Basin is characterized by Pantanal wetlands and the Paraguay and Paraná river floodplains, as well as

https://doi.org/10.5194/egusphere-2026-5245
Preprint. Discussion started: 28 September 2026

extensive urban and agricultural areas. Methane emissions in the Paraná Basin are driven by anthropogenic activities in cities and by livestock in surrounding rural regions. Note that Hancock et al. (2025) present individual wetland methane estimates for the Pantanal (1.3-1.6 Tg CH_4 yr^{-1}) and the Paraná (2.0-2.1 Tg CH_4 yr^{-1}), while Gloor et al. (2021) report for the Pantanal (2.0-2.8 Tg CH_4 yr^{-1}). Therefore, despite their relevance, these two basins (i.e. Orinoco and Paraná) are still under-researched and require further investigation.

Global atmospheric inversions combine atmospheric observations with transport models to estimate surface methane emissions. However, there is a lack of studies that assess the skill of global inversions assimilating in-situ data across South America in constraining the methane fluxes of these three river basins. Particularly for regions where observational coverage is sparse, global inversion systems may be more sensitive to system configuration and prior assumptions than to the underlying atmospheric signal. Belikov et al. (2026) provided a compelling illustration of this sensitivity, showing that the choice of hydroxyl radical (OH) field alone (climatological versus interannually varying) leaves global emissions essentially unchanged while shifting regional estimates by 10–20% across continents. Similarly, (Zhao et al., 2020) demonstrated that different prescribed OH distributions can substantially alter inferred regional methane emissions, with tropical South America identified as one of the region's most sensitive to OH uncertainties. Characterizing such structural sensitivity is essential before regional estimates from global inversions can be interpreted with confidence in data-limited regions.

In this study, we use the Jena CarboScope global inversion system (Rödenbeck, 2005; Basso et al., 2026, adapted for CH_4) to estimate the methane budget, seasonal cycle, and interannual variability across the Amazon, Orinoco, and Paraná river basins for the 2010–2019 decade. CarboScope has been configured to assimilate the aircraft vertical profiles at Santarém (SAN), Alta Foresta (ALF), Rio Branco (RBA), Tabatinga (TAB) and Tefé (TEF) (Basso et al., 2021) together with the Amazon Tall Tower Observatory (ATTO) record (Botía et al., 2020; Van Asperen et al., 2023) (Fig.1). These six in-situ constraints are concentrated in the Amazon basin and have not been jointly used in previous global inversion intercomparisons of South America. We exploit this configuration to answer three questions: (i) What constraint does the global atmospheric network alone place on the methane budget of the three basins? (ii) What is the added value, if any, of assimilating Amazon in-situ data on the budget of the Amazon itself

https://doi.org/10.5194/egusphere-2026-5245
Preprint. Discussion started: 28 September 2026

and, critically, on the budgets of the neighbouring Orinoco and Paraná basins? (iii) How do our estimates compare with other state of the art inversion systems?

2 Methods

2.1 The CarboScope Inversion system

The CarboScope inversion system estimates the fluxes of atmospheric trace gases by assimilating atmospheric mole fraction observations within a Bayesian inversion framework (Rödenbeck, 2005). This Bayesian framework combines prior information with atmospheric methane observations and accounts for the uncertainty in both (i.e. observations and priors) to optimize the surface-atmospheric fluxes. The inversion optimizes fluxes on a daily time scale. The transport model in CarboScope is TM3 (Heimann and Körner, 2003), run here at a horizontal resolution of 5° × ~3.8° (longitude x latitude) and 19 vertical layers extending from the surface to the lower stratosphere (Rödenbeck, 2005). As meteorological input to TM3, we used the reanalysis from National Center for Environmental Prediction (NCEP) (Kalnay et al., 1996).

The inversion was performed for the 2001–2020 period, which includes a three year spin-up period (2001–2003) and a one year spin-down period (2020). Our main focus is the period 2010-2019, which overlaps with the period having most of the data coverage in the Amazon. This period also coincides with one of studied references in the Global Methane Budget (Saunois et al., 2025). Within the Bayesian framework, the optimal state vector is obtained by minimizing the cost function which consists of the observational constraint term and the prior constraint term. We use the Conjugate Gradient descent algorithm with re-orthonormalization for optimizing the cost function and perform 115 iterations until it reaches a minimum. A detailed description of the cost function and its optimization can be found in the CarboScope technical report (Rödenbeck, 2005). The spatial error correlation length scale has been set to 1000 km in both the latitude and longitude directions for all flux categories, while temporal correlations are applied at approximately 15 days resolution. The prior methane flux is

https://doi.org/10.5194/egusphere-2026-5245
Preprint. Discussion started: 28 September 2026

separated into four source categories (wetlands, anthropogenic, biomass burning, and other natural sources), each assigned an independent prior uncertainty. This allows the inversion to optimize the source categories independently. Where multiple source categories coexist within the same grid cell, the posterior adjustment is allocated among the individual source categories according to their respective prior uncertainties.

The total model-data mismatch uncertainty is defined as the sum of squares of the model and observational uncertainty components. Observational uncertainty is smaller compared to the estimated transport error and assumed 3 ppb for all observations. The model uncertainty is considered by scaling the 35 ppb (σ_{mod}) transport error by a factor, which is applied to different classes of sites, as described in the Table A1. To ensure a balance between sites with different measurement frequency, we apply a data density weighting (Rödenbeck, 2005). In particular, the ATTO tower observations are available at hourly resolution, whereas aircraft observations are typically available twice per month. Following the setup of Botía et al. (2025) for a regional CO_2 inversion using the same stations over South America, to avoid overweighting high-frequency observations, the uncertainty assigned to individual measurements is inflated by a factor of $\sqrt{N_{hours/week}}$ for the hourly ATTO data and by $\sqrt{N_{flask/profile}}$ for the aircraft measurements, where N_{hours} is the number of observations within a given week and N_{flask} is the number of flask measurements per profile, which are taken on average twice per month. This ensures that all stations are of the same weight in the inversion (Rödenbeck, 2005).

Posterior uncertainties derived from the inversion are commonly referred to as Bayesian uncertainties. These uncertainties are obtained from the posterior covariance matrix, which combines information from the prior flux uncertainties and the observational error covariance matrix (Rödenbeck, 2005). The magnitude of the posterior uncertainty primarily depends on the availability and density of observations, as well as on the assumed uncertainties in the prior fluxes and the model–data mismatch.

https://doi.org/10.5194/egusphere-2026-5245
Preprint. Discussion started: 28 September 2026

Posterior uncertainties in this study are calculated separately for each basin and for each year over the period 2010–2019. The uncertainty reduction achieved by the inversion is quantified as

$$\Delta \sigma = 1 - \frac{\sigma_{posterior}}{\sigma_{prior}}$$

where σ_{prior} and $\sigma_{posterior}$ denote the prior and posterior uncertainties, respectively.

2.1.1 Prior fluxes

The prescribed prior flux categories in our setup are wetlands, anthropogenic emissions, biomass burning (fire), other natural emissions (e.g. termites, herbivory (wild ruminant), natural geological emission) and ocean emissions. For the wetland prior, we use the emissions from the WetCHARTs ensemble (Bloom et al., 2017) for the period 2001-2019. WetCHARTs provides the fluxes at a spatial resolution of 0.5° × 0.5°. The WetCHARTs dataset provides estimates of wetland methane emissions based on different definitions of wetland extent, global scaling factors, and temperature sensitivity of methane production. In this study, we use the extent parameter 3 (EP3), which is based on ERA interim precipitation and the Global Lakes and Wetlands Database (Lehner and Döll, 2004). For the rest of the ensemble setup, we selected the intermediate WetCHARTs global scaling factor (166 Tg CH_4 yr^{-1}) from the three available values (124.5, 166, and 207.5 Tg CH_4 yr^{-1}). In WetCHARTs, heterotrophic respiration is modeled using CARDAMOM (model 9 from the MsTMIP ensemble) (Huntzinger et al., 2026). The Q_{10} parameter represents the temperature sensitivity of methane production (CH_4:C), with values of 1, 2, and 3. In this ensemble approach, we used the mean of these three Q10 values. For more detailed information on WetCHARTs please refer to Bloom et al. (2017).

Monthly mean emissions of biomass burning (fire) were taken from the Global Carbon Project (Saunois et al., 2025). Anthropogenic emissions were sourced from the EDGAR v8 inventory (Crippa et al., 2021), which encompasses contributions from agriculture, livestock, waste management, and fossil fuel exploitation. Other natural emissions included geological sources (Etiope et al., 2019), as well as contributions from termites and herbivory (wild ruminant), with

https://doi.org/10.5194/egusphere-2026-5245
Preprint. Discussion started: 28 September 2026

monthly values obtained from the JSBACH model (Kleinen et al., 2020). Finally, global ocean emissions were based on Weber et al., (2019), using an annual mean methane flux repeated throughout the year (i.e., no seasonal cycle) for both diffusive and ebullitive processes (Basso et al., 2026).

We assign prior emission uncertainties separately for each emission category, including wetlands, anthropogenic emissions, biomass burning, ocean, and other natural sources. The category-specific uncertainties at yearly scale described in Table 1. We optimize two temporal components for wetlands, wetlandsS for the seasonal component and wetlandsI for the interannual variability (IAV). The motivation for optimizing a seasonal and an inter-annual component individually is the assumption that the seasonal amplitude in fluxes is larger than the wetlands' IAV in the region of interest, which can be implemented by choosing different a-priori uncertainties for these separate components. The resulting posterior components combined are then representing the total posterior wetland flux. The resultant global total uncertainty in prior total methane flux is 43.55 Tg CH_4 yr^{-1}.

Table 1. Category-specific prior globally integrated uncertainties at yearly scale.

Source Category	**Uncertainty (Tg CH_4 yr^{-1}) at yearly scale**	**Uncertainty (% of Annual flux)**
wetlandsS	± 19.67 Tg CH_4 yr^{-1}	12.02 %
wetlandsI	± 19.28 Tg CH_4 yr^{-1},	11.77%
anthropogenic	± 31.46 Tg CH_4 yr^{-1}	9.08 %
Other	± 5.19Tg CH_4 yr^{-1}	8.26 %
Biomass burning	±1.92 Tg CH_4 yr^{-1}	14.12 %

2.1.2 Observational constraint and study regions

We assimilate atmospheric observations from 154 surface and aircraft measurement sites worldwide (Fig. 1). Most observational data used in this study were accessed through NOAA

https://doi.org/10.5194/egusphere-2026-5245
Preprint. Discussion started: 28 September 2026

GML ObsPack v6.0 (Schuldt et al., 2025), the ICOS Carbon Portal (ICOS RI et al., 2024) , and the World Data Centre for Greenhouse Gases (WDCGG) database (https://doi.org/10.50849/WDCGG_CH4_ALL_2023). Detailed information on the assimilated observations can be found in Basso et al. (2026). This global network includes six stations located in the Amazon Basin consisting of five aircraft based sites and the ATTO station. Aircraft observations were taken from the same five sites as in Basso et al. (2021), with data available at (https://doi.org/10.1594/PANGAEA.926834) (Gatti et al., 2021). These vertical profile measurements of atmospheric gases were made across the Brazilian Amazon basin from 2010 to 2018. Data were collected at the following sites (Fig.1): Alta Floresta (ALF, 56.7°W, 8.9°S), Rio Branco (RBA, 67.9°W, 9.3°S) from 2010-2018, Santarém (SAN, 55.0°W, 2.9°S) from 2004-2018, Tabatinga (TAB, 69.7°W, 6.0°S) from 2010-2012 and Tefé (TEF, 3.7°S, 66.5°W) from 2013-2018 (Basso et al., 2021). Since the TAB station was replaced by TEF in 2012, both sites were treated as a single station (TAB-TEF) in the inversion. Aircraft measurements were assimilated as individual flask samples using the full vertical profile.

Apart from the five aircraft sites, we added the data from ATTO (Fig.1). ATTO is situated within the Uatumã Sustainable Development Reserve, which is 150 km northeast of Manaus (Andreae et al., 2015). It consists of a 325 m tower and several 80 m towers with instruments for measurement of aerosol, trace gas, and greenhouse gases. The record of methane at ATTO site started March 2012 with half-hourly measurements. The 80-meter towers are instrumented at five different levels (79m, 58m, 34m, 24m, 4m), and each level is measured by 2 cavity-ring down spectroscopy instruments, manufactured by Picarro Inc. In this CarboScope inversion, only observations from the 79 m height were assimilated. For the inversion we average the 30-min values to hourly observations and assimilate only daytime (17:00 to 21:00 UTC) observations.

https://doi.org/10.5194/egusphere-2026-5245
Preprint. Discussion started: 28 September 2026

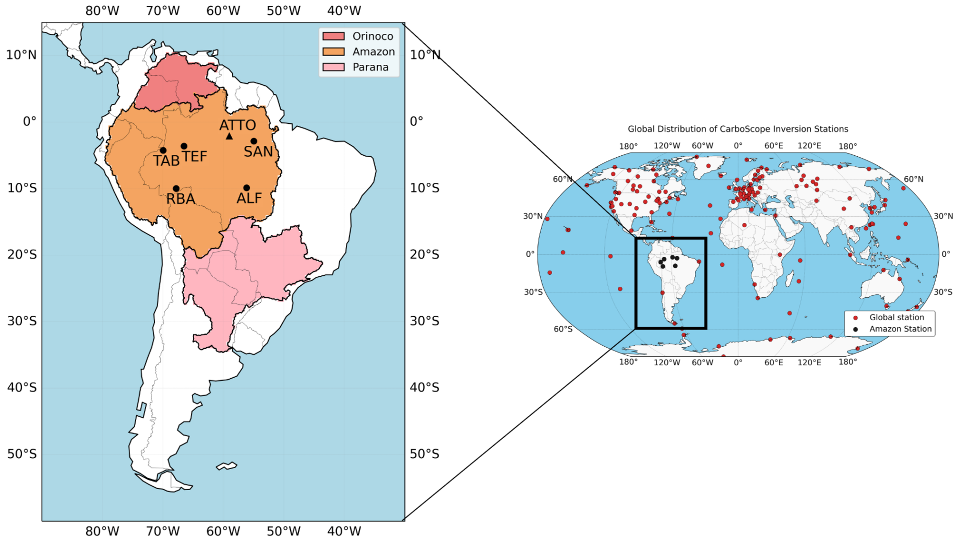

Figure 1.Global observational network used in the CarboScope inversion framework with a zoom over south America to highlight the Amazon basin observation network. Black dots indicate Amazon aircraft measurement stations and black triangle the ATTO site. The coloured areas show the river basin boundaries used for methane flux integration and analysis (derived from the HydroBASINS dataset, Lehner and Grill, 2013).

In this study we focus specially on three river basins in South America: the Orinoco, Amazon and Paraná (Fig. 1)**.** The Orinoco basin is situated at the north end of South America with a total area of 0.94 x 10^6 km^2. The annual rainfall ranges from 1000-4000 mm depending upon the location (Builes-Jaramillo et al., 2024). The Orinoco basin is characterised by a strong seasonal unimodal inundation pattern, primarily driven by rainfall during the wet season (May to October) (Frappart et al., 2014). The Amazon River Basin is the largest river basin of the three, covering approximately 5.88 × 10^6 km² and extending across seven South American countries. The Amazon basin experiences a mean annual precipitation of approximately 1500 mm to 3000 mm yr^{-1} (Drumond et al., 2014), but having regional differences mainly in dry season length. Maximum inundation in the Amazon basin typically occurs during May-June (Alsdorf et al., 2000; Hess et al., 2015). Lastly, we consider the Paraná basin, which is located south of the Amazon basin with an estimated area of 2.64 x 10^6 km^2. The annual precipitation in the Paraná ranges from 1550 to 2125 mm yr^{-1} depending on the region. Inundation patterns

https://doi.org/10.5194/egusphere-2026-5245
Preprint. Discussion started: 28 September 2026

(especially in the Pantanal floodplain) show that flooding occurs during the wet season (October-March) (Caldana et al., 2021; Nascimento et al., 2023). Throughout this study, the Paraná basin refers to the entire Paraná River basin, including the Paraguay River basin and the Pantanal wetlands.

2.1.3 Atmospheric methane sink

The total methane sink consists of soil uptake and chemical loss in the atmosphere. Tropospheric oxidation occurs through the reaction of methane with hydroxyl (OH) radicals; in this study the corresponding oxidation fields are taken from the Spivakovsky et al. (2000) dataset. In the stratosphere, methane undergoes reactions with OH, Cl, and O(1D), as modeled by the ECHAM5/MESSy1 framework (Jockel et al., 2006). Additionally, the tropospheric chlorine sink is simulated based on the findings of Hossaini et al. (2016). Soil uptake of methane is modeled as a zeroth-order reaction in the surface layer, utilizing microbial oxidation rates from the LPJ-Bern model (Spahni et al., 2011).

2.2 Sensitivity tests

The CarboScope inversion configuration described so far represents our reference setup (REF, Table 2). This REF run uses the WetCHARTs EP3 wetland prior fluxes, the OH climatology is from Spivakovsky et al. (2000) dataset. It uses data from all six sites in the Amazon basin along with global observational constraints (as described in Sect. 2.1.2) and MDM uncertainty as described in Table A1. Aircraft measurements were assimilated as individual flask samples using the full vertical profile. This configuration serves as the baseline against which all sensitivity experiments are evaluated.

In this study we perform a series of sensitivity experiments with the CarboScope inversion system to assess how different inversion settings influence the estimated fluxes. The experimental design is broadly divided into two categories. The first category focuses on varying prior flux estimates, particularly wetland emissions, to assess how different prior assumptions influence posterior methane fluxes. In the second category, we investigate the

https://doi.org/10.5194/egusphere-2026-5245
Preprint. Discussion started: 28 September 2026

effect of different ways for assimilating the observational data. In all sensitivity experiments, only the tested factor was varied while all other settings were kept unchanged as in the REF setup. We analyse the spread between different experiments to assess the variability in methane emission for different inversion setups. In addition to these categories, the role of the different chemistry field is analyzed in a separate experiment in which we used an additional chemistry field from Patra et al. (2011). In the following section, each experiment is described in detail, and summarised in Table 2.

2.2.1. Sensitivity experiments varying the prior emissions x_b

Wetland prior fluxes (ST_{WET}). In addition to the REF inversion setup using WetCHART EP3, we use two other models from the WetCHARTs ensemble (Bloom et al., 2017) to assess the sensitivity of the inversion to prior assumptions. We used a WetCHARTs-based prior with an alternative wetland extent that combines ERA-Interim precipitation with GLOBCOVER land cover data (extent parameter 4, EP4). Additionally, we used the LPJ-wsl (Zhang et al., 2023; DOI https://zenodo.org/records/7595223) as another prior emission model for the wetlands. LPJ-wsl is a process-based land surface model designed to simulate the fully coupled carbon and water cycles of the terrestrial biosphere and is based on the LPJ dynamic global vegetation model framework (Calle and Poulter, 2021). The wetland methane fluxes used here are provided at a spatial resolution of 1° × 1°.

2.2.2 Chemistry setup (ST_{CHEM}). We conduct a sensitivity experiment using an alternative atmospheric chemistry field. This alternative chemistry setup uses climatological three-dimensional monthly OH and $O(^1D)$ fields distributed as part of the TRANSCOM methane inversion experiment (Patra et al., 2011). The OH field combines the semi-empirical tropospheric OH distribution of Spivakovsky et al. (2000), reduced by 8% following Huijnen et al. (2010) with a two-dimensional model-simulated stratospheric OH distribution, as described by (Patra et al., 2011). In addition, climatological chlorine fields for both the troposphere and stratosphere are adopted from Wang et al. (2021).

https://doi.org/10.5194/egusphere-2026-5245
Preprint. Discussion started: 28 September 2026

2.2.3 Sensitivity experiments with assimilated data (y)

Leave-One-Out Station Experiment (ST_{LOO}) In this experiment, one station within the Amazon Basin was excluded from the inversion at a time and the inversion was run again. With this, we assess the effect of individual stations on the posterior fluxes in South America.

Excluded all Amazon Basin stations (ST_{-ALL}). In this sensitivity experiment, all atmospheric observation sites located within the Amazon Basin were excluded from the inversion. This experiment was designed to quantify the contribution of the Amazon atmospheric observing network to constraining regional methane emission estimates and to assess how strongly the inversion relies on regional observations.

Only ATTO station (ST_{only_ATTO}). In this sensitivity experiment, the inversion was performed using observations only from the ATTO station within the Amazon Basin, while excluding all other Amazon observational sites. This experiment was conducted to quantify the extent to which the ATTO measurements alone constrain the posterior methane flux estimates.

Vertical Profile Representation (ST_{VPR}) Aircraft observations provide information throughout the atmospheric column up to ~4.5 km height, making them suitable for partial column assimilation. This experiment assesses the sensitivity of posterior methane fluxes by varying how the aircraft profiles were assimilated in the inversion. The REF inversion, the full profile case, each individual observation in each vertical profile was assimilated. The first sensitivity case (ST_{VPR1}) assimilates a mass-weighted average over all the data points in the aircraft profile (i.e. a partial xCH_4 column average). The second sensitivity case is a split profile (ST_{VPR2}), in which the profile was divided at 2500 m and represented by two mass-weighted partial XCH_4 observations: one for the profile below 2500 m and one for the profile above 2500 m and both partial columns are assimilated in inversion. In the ST_{VPR2} experiment, we used 2500 m as the threshold to ensure that the partial column is above the convective boundary layer.

Model-data mismatch (MDM) Assumptions (ST_{MDM}). The impact of the model-data mismatch (MDM) uncertainty on the inversion was tested in a sensitivity experiment by assuming a homogeneous observational uncertainty of 35 ppb (σ_{mod}) for both aircraft and tall-tower observations. This is compared against the REF setup of the CarboScope-CH4 system, where different MDM uncertainties are applied for different observation types (aircraft: 35 ppb; towers: 105 ppb). This test is used to assess the impact of observational weighting assumptions on the inversion estimates.

Table 2. Summary of sensitivity experiments and corresponding modifications relative to the REF setup in the CarboScope inversion.

ID	What changed relative to REF setup	Sub experiment Id
REF	Baseline inversion setup	
ST_{WET}	Alternate wetland priors use	ST_{WET1} (WetCHART EP4) ST_{WET2} (LPJ-WSL)
ST_{CHEM}	Alternate chemistry field uses	
ST_{LOO}	Exclude one station at a time from the Amazon basin	$ST_{-ALF,}$ ST_{-RBA} ST_{-SAN} ST_{-TAB_TEF} ST_{-ATTO}
ST_{-ALL}	Exclude all the stations from the Amazon basin	
ST_{Only_ATTO}	Only data from ATTO station is assimilated in inversion	
ST_{VPR}	Different way of vertical profile representation	ST_{VPR1} (Avg. profile) ST_{VPR2} (Vertical profile split at 2500m)
ST_{MDM}	Apply uniform (35 ppb) MDM uncertainty to aircraft and tower measurement.	

2.3 Inversion systems used for intercomparison

To assess our posterior fluxes, we compared our results to fluxes from the following inversion systems: CAMS-CH_4 version v2022r2 (Bergamaschi et al., 2013), CarbonTracker-CH_4-2023 (Oh et al., 2023), and TOMCAT/INVICAT (Wilson et al., 2021). These inversion systems differ in the assimilated observational data, atmospheric transport models, prior fluxes, atmospheric methane loss processes, and inversion methodologies. A comparative analysis of

https://doi.org/10.5194/egusphere-2026-5245
Preprint. Discussion started: 28 September 2026

methane budgets across these systems therefore provides an assessment of uncertainty in the methane budget for the major South American river basins. For a brief description of each inversion system, we refer the reader to Appendix B. In Table 3 we provide a summary of the main differences of each system. It is worth mentioning that one of the systems (i.e. CarbonTracker-CH_4) assimilated $\delta^{13}C$–CH_4 measurements from several stations of the global monitoring network. Furthermore, CarbonTracker-CH_4 and CarboScope include methane in-situ observational constraints from the Amazon region, whereas the TOMCAT and CAMS (in-situ+Satellite) inversions include GOSAT satellite measurements over global scale. CAMS (in-situ) is the only inversion system which does not use measurements from the study region, but only assimilates background stations. CarboScope is the only inversion system which assimilates the in-situ methane data from ATTO. Please note that three of the inversion systems (CarboScope, CarbonTracker and CAMS) use closely related TM3/TM5 transport models, which may partly explain the similarities among their results.

Table 3. Summary of all inversions used in this study, including their prior emission and type of observational data.

Inversion	**Jena CarboScope**	**CarbonTracker-CH_4**	**TOMCAT**	**CAMS (v2022r2)** **Surface , satellite + surface**
Prior fluxes				
Wetlands	WetCHARTs	TEM	Jules Model (Clark et al., 2011)	LPJ-wsl with CRU and MERRA2 reanalysis dataset
Anthropogenic	EDGAR v8	EDGAR v4.3.2	EDGAR v4.2	EDGAR v7.0
Biomass burning	GFED 4.1s	GFED4.1s	GFEDv4.2	ACCMIP-MACCity inventory +GFAS

https://doi.org/10.5194/egusphere-2026-5245
Preprint. Discussion started: 28 September 2026

CH_4 Loss Processes (Sinks)	Tropospheric oxidation: OH (Spivakovsky et al., 2000) scaled to CH_3CCl_3 lifetime; Cl (model derived estimates) Stratospheric oxidation: OH, Cl, O(1D) (monthly climatology from ECHAM5/MESSy1) Tropospheric chlorine sink: Hossaini et al., (2016) Soil uptake: Zeroth-order microbial oxidation (Spahni et al., 2011)	Atmospheric chemical sink (OH, O(1D), Cl): Prescribed from ECHAM5/MESSy1 (Jockel et al., 2006) OH fields scaled to methyl chloroform (Spivakovsky et al., 2000) Tropospheric Cl: Hossaini et al., (2016) Soil sink: TEM (Zhuang et al., 2013; Liu et al., 2020)	Tropospheric OH oxidation: monthly climatological OH fields from Spivakovsky et al. (2000) , Patra et al. (2011) and scaled by 8% Hossaini et al., (2016). Stratospheric oxiation: monthly CH_4 loss due to Cl and O(^{1}D) from TOMCAT full-chemistry simulations (Monks et al., 2017)	Tropospheric loss via OH radicals (CAMS reanalysis) Stratospheric loss via OH, Cl, and O(1D) from ECHAM5/MESSy1 (Jockel et al., 2006)
Observation type	In-situ surface flask & measurements from 154 stations. NOAA GML ObsPack, the ICOS Carbon Portal and the World Data Centre for Greenhouse Gases (WDCGG) database .	Atmospheric CH_4: NOAA GML GLOBALVIEW plus v7.0 (1983–2023) $\delta^{13}C$-CH_4 isotopes: INSTAAR & 6 labs (1991–2023)	Surface and Satellite observations: NOAA, GOSAT XCH_4 (University of Leicester Proxy) (Parker et al., 2020)	NOAA surface observations, GOSAT satellite CH_4 retrievals; surface-only (CAMS) or combined inversion versions (CAMS-Satellite)

https://doi.org/10.5194/egusphere-2026-5245
Preprint. Discussion started: 28 September 2026

Transport Model & Meteorology	TM3 model; Meteorology: NCEP from 1950; Resolution 5° × ~3.8°; 19 vertical layers.	TM5 model; ERA-Interim (pre-2019), switched to ERA5 (post-2019); Resolution 3° × 2°; 25 vertical layers	TOMCAT 3-D Eulerian offline CTM; ERA-Interim reanalysis (1979–2019), Resolution 5.6° × 5.6°; 60 layers	TM5 model; ERA5 reanalysis; 34 layers; Resolution 1° × 1°
Observational Constraint from in-situ or flask data in the Amazon basin	Yes	Yes	No	No

Because the inversion systems use different native horizontal resolutions, basin-integrated methane emissions were calculated using fractional basin masks generated on the native grid of each inversion system. The fractional masks were obtained by intersecting the basin polygons with the native model grid, such that each grid cell contributed according to the fraction of its area located within the basin (Fig A1). Basin emissions were then calculated by weighting the grid-cell methane fluxes by these fractional areas before spatial integration. The resulting basin areas for each inversion system are summarized in Table 4. Despite differences in native model resolution, the resulting basin areas differ by less than approximately 4% among the inversion systems, indicating that all systems represent essentially the same spatial domain.

Table 4. Effective basin areas (km²) of the native-grid fractional masks used for basin-integrated methane emission calculations in each inversion system.

Inversion System	**Orinoco (km²)**	**Amazon (km²)**	**Parana(km²)**
CarboScope	0.955×10^6	5.99×10^6	2.68×10^6
CarbonTracker	0.937×10^6	5.88×10^6	2.64×10^6
TOMCAT	0.941×10^6	5.91×10^6	2.65×10^6
CAMS	0.918×10^6	5.89×10^6	2.67×10^6

2.4 Evaluation of posterior mole fractions with independent datasets

The performance of all global inversion systems used in this study, i.e. CarboScope, CAMS, TOMCAT, and CarbonTracker, were evaluated using independent methane mole fraction data not assimilated in any of the inversion systems. These independent stations are Manaus (MAN, 2.5°S, 59.8°W), Pantanal (PAN, 9.45°S, 56.4°W), ATTO (2.14°S, 58.99°W) and Porto Velho (PV, 8.77°S, 63.87°W). The data from MAN consist of aircraft-based in-situ measurements of methane during vertical profiling flights, using a Picarro CRDS analyzer from near the surface to up to ~5km (Miller et al., 2023). At PAN there are aircraft-based vertical profiles, where air is sampled in flasks during the aircraft descent from about 4.4 km altitude to near surface, and later analysed in the laboratory for dry-air mole fractions (Gloor et al., 2021). The measurements of methane at the Porto Velho site were taken using a Fourier transform infrared (FTIR) Bruker 125M spectrometer, in the NDACC-IRWG configuration (https://www2.acom.ucar.edu/irwg). Methane total columns and low-vertical resolution profiles (degrees of freedom for signal DOFS of about 2-2.5) are derived from solar absorption spectra (see details in, e.g., Zhou et al., 2018)). The following Table 5 summarizes the inversion systems evaluated, along with the corresponding observational sites. For the MAN and PAN aircraft observations, the evaluation was performed separately for measurements below 2 km, which are most sensitive to surface methane emissions, and above 2 km, representing the free troposphere where methane mole fractions are more strongly influenced

https://doi.org/10.5194/egusphere-2026-5245
Preprint. Discussion started: 28 September 2026

by vertical mixing and long-range transport. At ATTO (Andreae et al., 2015) , only the 79 m measurement level was available for evaluation, which is also representative of near-surface methane emissions. For the PV's FTIR observations, the evaluation was based on the methane total column, as the retrieval provides only limited vertical information (only about 1 DOFS in the surface-12km range). For CarboScope, atmospheric methane mole fractions simulated using both prior and posterior fluxes were available for evaluation. For TOMCAT, CAMS, and CarbonTracker, only mole fractions simulated using posterior fluxes were available.

Table 5. Overview of inversion systems evaluated against different observational sites and the corresponding time periods used for each comparison.

Site	Inversion systems evaluated	Time period
MAN	CAMS, CarboScope, TOMCAT, CarbonTracker	2017-2019
PAN	CAMS, CarboScope, TOMCAT	2017-2019
ATTO	CAMS, CarbonTracker, TOMCAT, CarboScope inversion without ATTO data (ST_{-ATTO})	2012-2019
PV	CAMS, CarbonTracker, TOMCAT, CarboScope	2016-2019

2.5 Statistical metrics

2.5.1 Anomaly calculation. Monthly methane flux anomalies were calculated for the period 2010–2019 for both the prior and posterior flux estimates for total South America and three river basins, Orinoco, Amazon and Paraná. A monthly climatology was first calculated by averaging the monthly methane fluxes for each calendar month over the period 2010-2019 ($F_{clim,m}$). The monthly anomaly was then calculated by subtracting the corresponding monthly climatological mean from the monthly methane flux,

$$A_{y,m} = F_{y,m} - F_{clim,m}$$

https://doi.org/10.5194/egusphere-2026-5245
Preprint. Discussion started: 28 September 2026

Where $F_{y,m}$ is the monthly methane flux for month (m) in year (y) and $F_{clim,m}$ is climatological mean for calendar month (m) and $A_{y,m}$ is corresponding methane flux anomaly. This removes the mean seasonal cycle and highlights the deviation from average monthly methane flux.

2.5.2 Ensemble mean and ensemble spread/ spread. For each sensitivity test, an ensemble of methane flux estimates was constructed by combining the REF inversion and all corresponding sub-experiments. The ensemble mean was calculated as the arithmetic mean of all ensemble members. The ensemble spread (or spread) was quantified as the standard deviation of the ensemble members, including the REF simulation and can be interpreted as the uncertainty in methane flux estimates introduced by varying a particular inversion setting in the sensitivity test.

2.5.3 Relative spread. To account for differences in methane flux magnitude among the river basins, the ensemble spread was also expressed as a percentage of the ensemble mean. The relative spread is calculated as

$$\text{Relative spread (\%)} = (\text{ ensemble spread } / \text{ ensemble mean }) \times 100$$

The relative ensemble spread provides a normalized measure of the sensitivity of the methane flux estimates, allowing direct comparison among sensitivity tests and river basins with different methane flux magnitudes.

2.5.4 Interannual variability (IAV) of the methane budget was quantified as the standard deviation of the annual mean methane fluxes across all years within the study period.

3 Results

3.1 Methane budget for the three river basins and impact of prior selection

Assimilating atmospheric observations into the CarboScope inversion leads to large adjustments in methane emissions across all three basins (Fig 2a). Despite the different wetland prior configurations, all experiments show the same qualitative posterior response after assimilating atmospheric observations, with methane emissions decreasing in both the Amazon and Orinoco basins and increasing in the Paraná basin. This demonstrates that atmospheric

https://doi.org/10.5194/egusphere-2026-5245
Preprint. Discussion started: 28 September 2026

observations constrain the direction of the posterior adjustment, while the magnitude of the adjustment remains dependent on the assumed wetland prior.

The Orinoco basin exhibits the largest posterior ensemble spread in the posterior methane budget, indicating the strongest sensitivity of the posterior methane budget to the choice of wetland prior. The ensemble mean (± posterior uncertainty) methane budget decreases from prior estimates (6.48 ± 1.32 Tg CH_4 yr^{-1}) to posterior estimates (4.44 ± 0.88 Tg CH_4 yr^{-1}) , with the ensemble spread increasing from 6.68% to 23.71% from prior to posterior (Fig 2a). Wetland emissions undergo the largest posterior adjustment **(**33–77%**)** (Fig A2). Because wetlands contribute more than half of the total methane budget, these large wetland adjustments directly propagate into the total posterior methane budget. The sparse observational coverage in this region makes the posterior methane budget more sensitive to the choice of wetland prior.

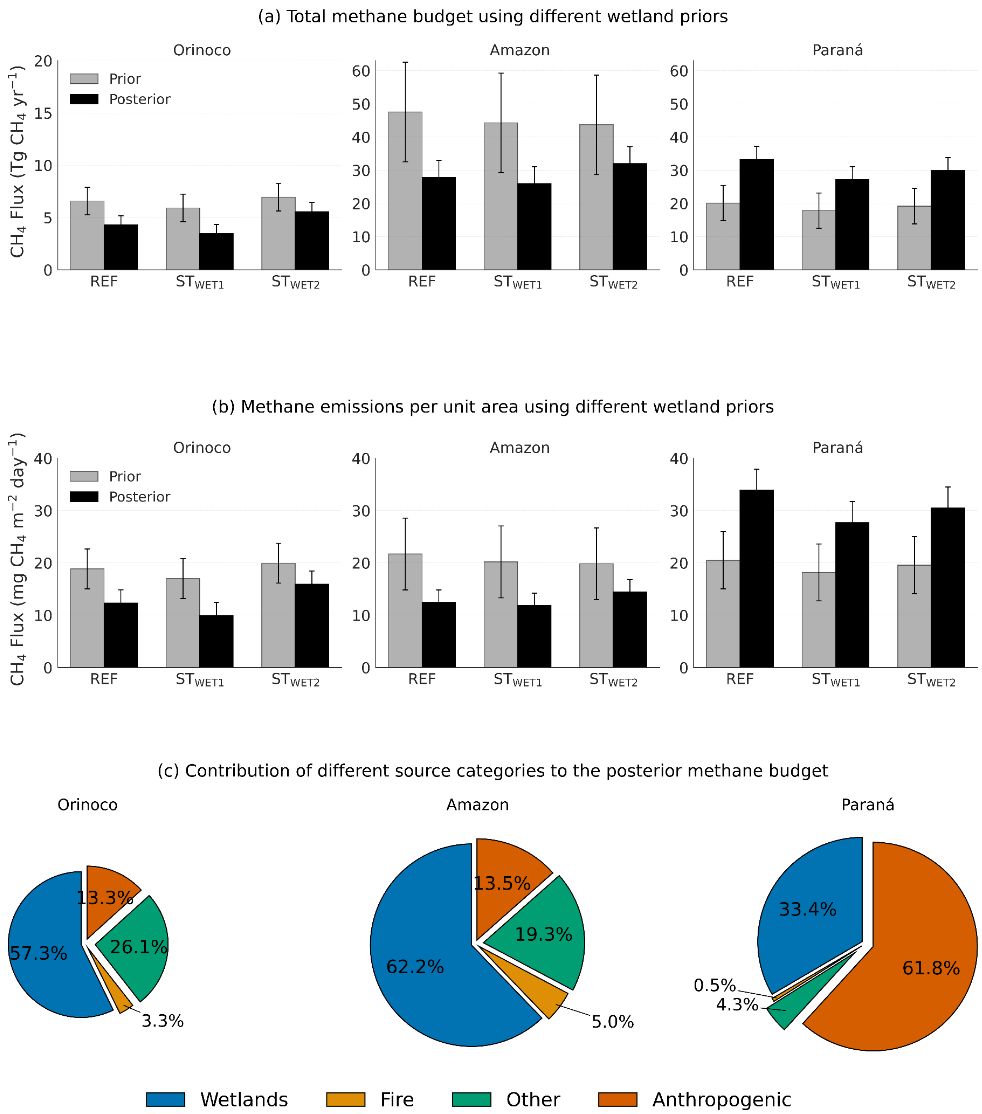

Figure 2. Total methane budget (2010–2019) from prior to posterior estimates for three South American river basins. (a) Pie charts showing the percentage contribution of each source to the posterior methane budget in each basin based on the mean across REF, ST_{wet1} and ST_{wet2}. (b) Total methane budget derived using different wetland prior assumptions in the CarboScope inversion system. (c) Total methane emissions expressed per unit area for inversions using different wetland priors. Error bars in panels b) and c) represent the posterior uncertainty in methane budget.

https://doi.org/10.5194/egusphere-2026-5245
Preprint. Discussion started: 28 September 2026

The Amazon basin shows a relatively small sensitivity of the posterior methane budget to the choice of wetland prior. The ensemble mean (± posterior uncertainty) methane budget decreases from prior estimate of 45.17 ± 14.99 Tg CH_4 yr^{-1} to a posterior estimate of 28.60 ± 5.45 Tg CH_4 yr^{-1}, while the ensemble spread increases only slightly from 3.86 % in the prior to 8.90 % in the posterior (see Fig 2a). Wetlands undergo the largest posterior adjustment (36–57%) (Fig A2) and largely control the reduction in the total methane budget. However, the comparatively small ensemble spread suggests that the Amazon observational network does provide constraints on the posterior methane fluxes.

In contrast, the Paraná basin is least affected by the choice of wetland prior. Although wetland posterior emissions increase by more than 100% in all three experiments compared to prior emission (Fig A2), the ensemble mean (± posterior uncertainty) methane budget changes from a prior estimate of 19.04 ± 5.33 Tg CH_4 yr^{-1} to a posterior estimate of 30.10 ± 3.95 Tg CH_4 yr^{-1} (Fig. 2a). The ensemble spread increased only modestly from 6.1% in the prior to 10.2% in the posterior This reflects the dominant contribution of anthropogenic emissions (~62%) to the total methane budget, which reduces the influence of wetland prior uncertainty on the basin scale methane budget.

Overall, these sensitivity experiments demonstrate that wetlands consistently undergo the largest posterior adjustments, but the influence of wetland prior selection on the posterior methane budget differs among the three basins. The posterior spread across the sensitivity experiments indicates that the Orinoco basin is the most sensitive to the wetland prior, whereas stronger observational constraints in the Amazon and the dominant anthropogenic contribution in the Paraná reduce this sensitivity.

A comparison of the ensemble mean methane emission per unit area (Fig. 2b, REF) shows distinct differences among the three river basins. The Paraná basin exhibits the highest methane flux density, increasing from prior emission 19.41 ± 5.45 to 30.68 ± 4.04 mg CH_4 m^{-2} day^{-1} in posterior fluxes following the inversion. In contrast, the Amazon basin shows substantially lower methane emissions per unit area, decreasing from 20.57 ± 6.86 to 12.91 ± 2.36 mg CH_4 m^{-2} day^{-1} . Similarly, the Orinoco basin decreases from 18.59 ± 3.80 to 12.73 ± 2.53 mg CH_4 m^{-2} day^{-1}. Notably, the posterior methane flux density in the Orinoco basin is nearly identical to that of the Amazon basin, indicating that despite its much smaller area, the Orinoco emits methane at a comparable rate per unit area.

https://doi.org/10.5194/egusphere-2026-5245
Preprint. Discussion started: 28 September 2026

The posterior methane budget of the inversion is dominated by different methane source categories across the three South American basins (Fig. 2c). Wetlands are the largest methane source in both the Amazon and Orinoco basins, contributing approximately 62% and 57% of the total methane budget, respectively. In the Amazon basin, anthropogenic emissions account for 13% of the total methane budget, while other natural sources (termites, herbivory (wild ruminants) and geological emissions) contribute 19%. A similar source partitioning is found for the Orinoco basin, where anthropogenic emissions contribute 13% and other natural sources account for 26% of the total methane budget. In contrast, methane emissions from the Paraná basin are dominated by anthropogenic sources, which contribute 62% of the total methane budget. Wetland emissions, primarily associated with the seasonally flooded Pantanal region, contribute 33%, while biomass burning remains a minor source (0.5%). Across all three basins, biomass burning contributes less than 5% of the total methane budget.

3.2 Sensitivity of methane emission estimates to inversion setups

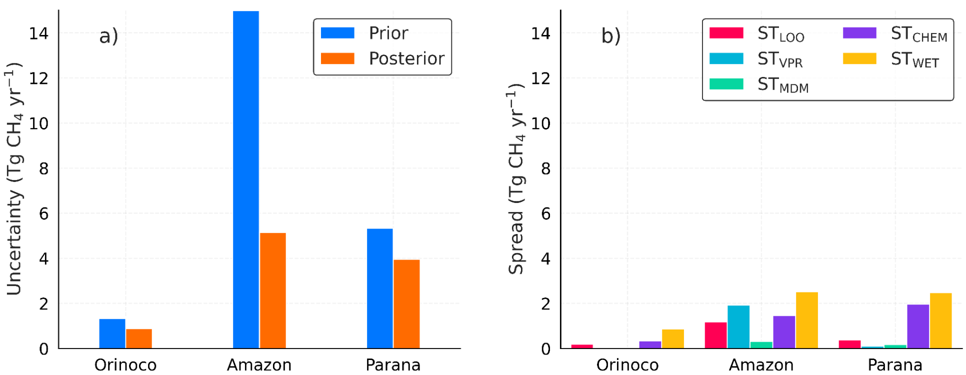

Figure 3. (a) Prior and posterior uncertainty from the inversion system. (b) Spread (see Sec 2.5.2) in posterior methane fluxes from the South American river basins across the sub-experiments of our sensitivity experiments (see Table 2 and Sec 2.2).

Across all three South American river basins, the assimilation of atmospheric observations leads to a clear reduction in uncertainty. The most pronounced reduction occurs in the Amazon basin, reflecting its relatively better observational coverage compared to the other two basins. The prior uncertainty (~15 Tg CH_4 yr^{-1}) for the Amazon basin decreases to ~5 Tg CH_4 yr^{-1} in

https://doi.org/10.5194/egusphere-2026-5245
Preprint. Discussion started: 28 September 2026

the posterior estimate (Fig. 3a), corresponding to a mean annual uncertainty reduction of ~66%. Although this value represents the average over the study period, the uncertainty reduction varies from year to year (Fig. A3, with SA data). In comparison, the Orinoco and Paraná basins have mean annual uncertainty reductions of only ~33% and ~25%, respectively. Note that our REF case including Amazon station data yields an uncertainty reduction of ~60–80%, whereas excluding them limits the reduction to ~40–50% in the Amazon basin (Fig. A3, without SA data). Note that the gain in uncertainty reduction added by the Amazon data in the Orinoco and Parana regions is less than 10%. For the Amazon the largest uncertainty reductions occurred during 2010–2012 when the full Amazon aircraft observing network was available. In contrast, weaker uncertainty reduction is seen during 2015–2016, coinciding with observational gaps, and again in 2019 when aircraft observations are unavailable and only ATTO data are assimilated. This demonstrates that Amazonian observations substantially enhance constraints on Amazon methane flux estimates, but to a lesser extent on the neighboring regions.

Here we consider the posterior uncertainty (Fig 3a) as the threshold above which varying a specific inversion setting leads to a significant variability in posterior fluxes. Removing individual Amazon observation sites (Fig 3b, ST_{LOO}) results in only small changes in the total methane budgets, with relative flux variations of ~4.2%, ~4.6%, and ~1.1% for the Amazon, Orinoco, and Paraná basins, respectively, all remaining within the estimated posterior uncertainty. To assess the importance of the regional observation network as a whole on basin methane emission, we performed the ST_{-ALL} experiment, in which all Amazon regional observations were removed simultaneously. Unlike the other sensitivity experiments, ST_{-ALL} is not included in the uncertainty analysis but serves as a diagnostic test of the role of the regional observational constraint. Removing the entire Amazon observation network increases the inferred Amazon methane emissions from ~28 to ~49 Tg CH_4 yr^{-1} (Fig A2, d)ST_{-ALL}), corresponding to an increase of approximately 75%. In contrast, the Orinoco methane budget increases by only 0.50 Tg CH_4 yr^{-1} (from 4.30 to 4.80 Tg CH_4 yr^{-1}; ~12%), while the Paraná basin exhibits the smallest response, with methane emissions decreasing slightly from 33.24 to 32.36 Tg CH_4 yr^{-1} (−2.6%). This demonstrates that the Amazon observation network provides a strong regional constraint on Amazon methane emissions, whereas its removal has only a limited influence on the inferred methane budgets of the neighbouring basins and even results in a small downward adjustment in the Paraná basin.

https://doi.org/10.5194/egusphere-2026-5245
Preprint. Discussion started: 28 September 2026

The rest of sensitivity tests performed (ST_{VPR}, ST_{chem}, ST_{mdm}) did not lead to significant changes in posterior fluxes as they resulted in a spread lower than the posterior uncertainty estimated for each region. In the ST_{VPR}, the Orinoco (4.30 - 4.40 Tg CH_4 yr^{-1}; ~0.95% relative spread) and Paraná (33.24 - 33.49 Tg CH_4 yr^{-1}; ~0.30% relative spread) basins are almost unaffected by different representations of the vertical profile. However, the Amazon basin shows a small sensitivity to profile representation, with a spread of ~2 Tg CH_4 yr^{-1} (~6% relative spread). The use of a different chemistry field (ST_{chem}) leads to emission reductions in Orinoco, Amazon, and Paraná basins by approximately 7%, 5%, and 6%, respectively compared to the REF case. Furthermore, varying the MDM uncertainty (ST_{mdm}) has only a minor impact on the posterior methane flux estimates. In the Amazon basin, the posterior flux changes by only 0.31 Tg CH_4 yr^{-1}, while in the Orinoco and Paraná basins the differences remain below 1%. Finally, the change in wetland prior (ST_{wet}) causes the largest relative spread in posterior estimates for the Orinoco basin, at around 20%, versus less than 10% for the Amazon and Paraná basins (Fig A4, ST_{WET}).

3.3 Seasonal variability in methane fluxes across regions

Posterior monthly methane fluxes in the Orinoco basin diverge substantially from the prior, indicating a strong observational constraint on the seasonal cycle. Posterior fluxes show a pronounced seasonal cycle with a seasonal amplitude of ~20 mg CH_4 m^{-2} day^{-1}: lower emissions during the dry season (Nov–Apr), reaching a minimum around April, and peaking in July during the wet season (May–Oct) (Fig. 4a). Wetland emissions dominate both the magnitude and seasonal amplitude of this signal (Fig. A5, REF). Fire emissions are also strongly seasonal, peaking in the dry season (Nov–Mar), but contribute only ~8.7% of the total. Other natural sources (termites, wild ruminants, geological seeps; ~26% of the total budget) and anthropogenic emissions (roughly constant year-round) show weak or no seasonality and do not shape the seasonal pattern. Removing individual Amazon stations has negligible effect on the posterior seasonal pattern, and even excluding all Amazon observations (ST_{-ALL}) largely preserves the seasonal shape, showing the global network constrains the timing of the cycle. However, the seasonal magnitude changes substantially without the regional network (ST_{-ALL}), producing unrealistic negative fluxes, particularly in April. Thus, while the Amazon network

https://doi.org/10.5194/egusphere-2026-5245
Preprint. Discussion started: 28 September 2026

helps prevent unrealistic negative fluxes, the mean magnitude of the seasonal cycle still remains more uncertain, as we will see next for the Amazon region.

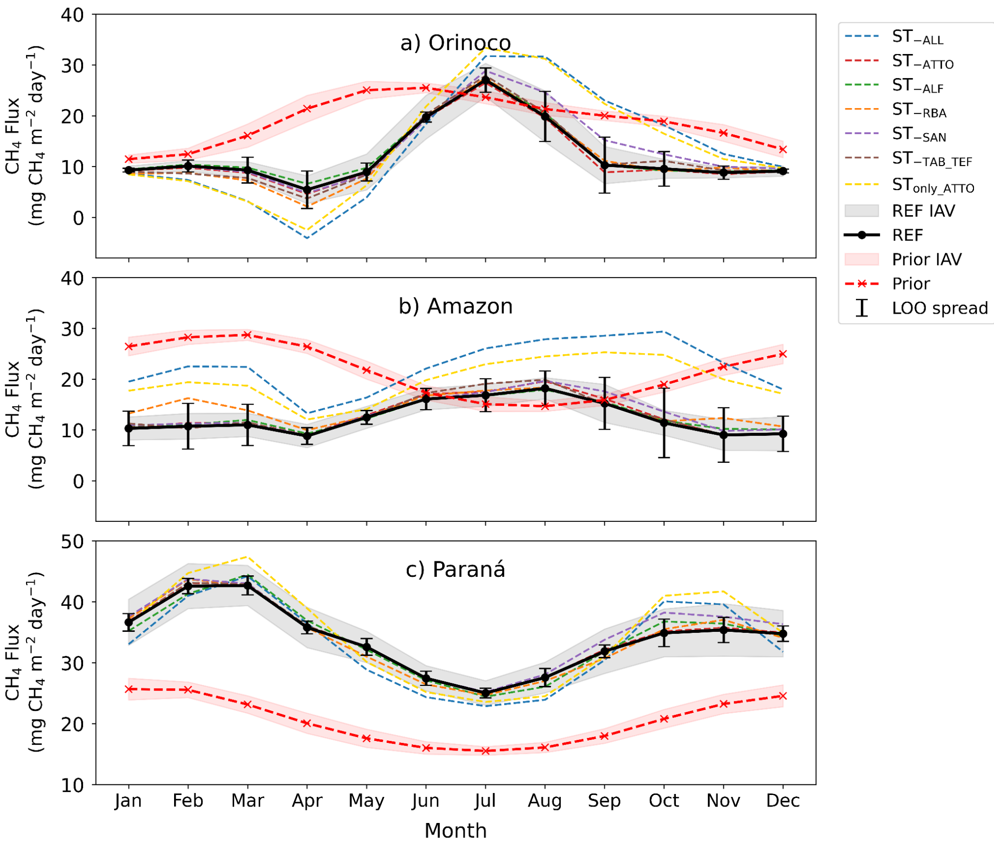

Figure 4. Seasonal cycle of CarboScope total CH_4 fluxes over the three South American river basins: a) Orinoco, b) Amazon, and c) Paraná basins. Results are shown for leave-one-out (LOO) experiments (dashed colored lines), in which individual stations are excluded from the inversion (a "–" indicates the station excluded in a given experiment), and for an inversion using only ATTO observations (dashed yellow line). These are compared with the REF inversion including all stations ("All", solid black line), where the shaded area represents the IAV. The prior flux estimate (red dashed line). Black bar represents the spread across the different LOO experiments.

A substantial change in methane seasonality is observed between prior and posterior flux estimates in the Amazon basin (Fig. 4b). Prior fluxes are highest during Dec–May and they are lowest during Jun–Nov, posterior fluxes instead peak in the dry season (August), highlighting the role of atmospheric observations in correcting the prior seasonal pattern. Wetland emissions remain the dominant driver of magnitude and seasonality in the posterior

https://doi.org/10.5194/egusphere-2026-5245
Preprint. Discussion started: 28 September 2026

estimates, but the August peak (Fig. 4b) reflects the combined contribution of wetlands, fires, and other natural sources (termites, wild ruminants, geological emissions). Fire emissions, though a small fraction of the total budget, are strongly seasonal, peaking in the dry season (August). The ST_{-ALL} experiment captures the overall seasonal pattern, but the seasonal peak occurs later, shifting from August in the REF case to October, indicating that the global network provides some constraint on the seasonal variability but not on the precise timing of peak emissions. Similarly, using only ATTO tower observations (ST_{only_ATTO}) still reproduces the seasonal phase, though the emission peak shifts later into the dry season. However, we find that the magnitude is far more sensitive to regional data, as the mean January emissions drop from ~20 mg CH_4 m^{-2} day^{-1} (ST_{-ALL}) to ~10 mg CH_4 m^{-2} day^{-1} (REF), confirming that regional observations are essential for quantifying emission magnitude, not just its timing. Removing individual stations, such as RBA, causes noticeable deviations early in the year, driven mainly by wetland emissions (Fig. A5, ST_{-RBA}), though no single station dominates the overall budget, the combined network provides the robust constraint.

In the Paraná basin, which hosts the Pantanal flooded savanna, we find a different response compared to the Amazon and Orinoco basins. After assimilating atmospheric observations, methane emissions increase relative to the prior estimate, and the seasonal cycle exhibits a larger amplitude, reaching approximately 15 mg CH_4 m^{-2} day^{-1}, with peak emissions occurring in the early months of the year (wet season). Although total methane emissions in the Paraná basin are dominated by anthropogenic sources, the seasonal cycle is primarily controlled by wetland emissions (Fig A5, REF). Fire emissions and other natural sources account for less than 5% of the total methane emissions from the basin. Despite their small contribution, these sources exhibit a distinct seasonal cycle, with emissions peaking during the dry season (April–Sep). The LOO experiments show that removing individual stations has little impact on the estimated fluxes, which remain close to the REF inversion. Even when all stations are removed (ST_{-ALL}), the resulting fluxes are still very similar to the REF case. This indicates that the Paraná basin is only weakly constrained by the available regional atmospheric observations network. However, the substantial differences between the prior and posterior fluxes indicate that global atmospheric observations still provide an important constraint.

3.4 Interannual variability

https://doi.org/10.5194/egusphere-2026-5245
Preprint. Discussion started: 28 September 2026

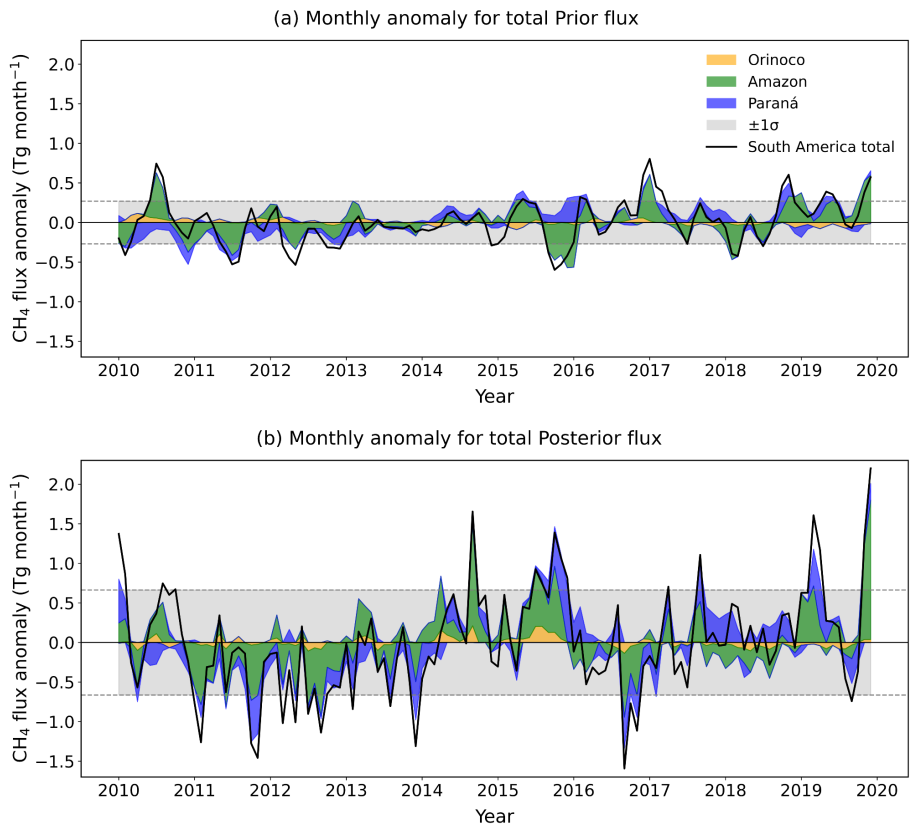

Figure 5. Time series of total methane emission anomalies (all sources included) for a) prior and b) posterior fluxes from 2010 to 2019 across the study basins.

Compared with the prior monthly methane flux anomalies, the posterior estimates exhibit substantially larger positive and negative departures from the climatological seasonal cycle, indicating enhanced IAV after assimilating atmospheric observations in inversion (Fig 5a,b). In addition to the larger anomalies, the posterior displays more frequent short positive and negative fluctuations than the relatively smooth prior, reflecting enhanced month-to-month variability introduced by the atmospheric observations. This increase is reflected in the standard deviation of the monthly anomalies, which increases from 0.27 Tg CH_4 month^{-1} in prior to 0.67 Tg CH_4 month^{-1} in posterior for South America. Similar increases in standard deviation from prior to posterior are observed for all three basins, with the largest relative increase occurring over the Paraná basin (0.10 to 0.26 Tg CH_4 month^{-1}), followed by the

https://doi.org/10.5194/egusphere-2026-5245
Preprint. Discussion started: 28 September 2026

Amazon (0.23 to 0.44 Tg CH_4 month^{-1}), while the Orinoco shows only a modest increase (0.03 to 0.04 Tg CH_4 month^{-1}).

The Amazon basin dominates inversion derived IAV of the continental methane budget throughout the study period. Monthly anomalies in the Amazon are strongly correlated with the total South American anomalies in both the prior ($r = 0.86$, $p < 0.05$) and posterior ($r = 0.83$, $p<0.05$), demonstrating that variability in continental methane emissions is primarily controlled by fluctuations over the Amazon basin. In contrast, the Paraná basin exhibits only a weak relationship with the South American anomalies in the prior ($r = 0.15$, $p < 0.01$), but this correlation increases substantially after inversion ($r = 0.62$, $p<0.05$), indicating a stronger contribution of Paraná variability to the continental methane anomaly in the posterior estimates. Owing to its comparatively small methane emissions, the Orinoco basin contributes little to the overall continental variability despite exhibiting a moderate positive correlation with the South American anomalies in posterior ($r = 0.50$, $p < 0.05$).

The inversion modifies not only the magnitude of the monthly methane flux anomalies but in many cases, it also modifies their phase relative to the climatological mean. Across South America, approximately 27% of the monthly anomalies transition from positive to negative values, or vice versa, between the prior and posterior estimates. This indicates that assimilating atmospheric observations changes whether individual months are estimated to have above- or below-average methane emissions relative to the monthly climatology. These transitions occur most frequently during 2015 and 2016, with six affected months in each year, and are predominantly associated with adjustments over the Amazon basin. An additional effect of the regional data is a reduction in the monthly anomaly magnitude. In the ST$_{\text{-ALL}}$ experiment we found that the overall temporal pattern of the monthly anomalies is similar to the REF case, but the magnitude is slightly larger (Fig A6).

While the monthly anomalies demonstrate that the inversion substantially enhances month-to-month methane variability, the annual mean methane fluxes (Fig. A7) provide insight into the year-to-year behaviour of the methane budget on annual timescales. The annual mean methane fluxes (Fig. A7) shows the Orinoco basin exhibits relatively small year-to-year variations, with

https://doi.org/10.5194/egusphere-2026-5245
Preprint. Discussion started: 28 September 2026

no clear long-term increase or decrease throughout the study period. Similarly, the Amazon basin does not show a persistent long-term trend, although annual methane emissions increase between 2011 and 2015 (+ 1.23 mg CH_4 m^{-2} day^{-1}), decline during 2015–2018 (-0.70 mg CH_4 m^{-2} day^{-1}), and again increase in 2019. In contrast, the Paraná basin displays a positive increase in annual methane emissions throughout the study period (+ 0.34 mg CH_4 m^{-2} day^{-1}). This increasing trend in the Parana basin is mainly attributed to wetlands (+0.16 mg CH_4 m^{-2} day^{-1}) and anthropogenic (+0.18 mg CH_4 m^{-2} day^{-1}) emissions.

A notable feature common to all three basins is the reduction in annual methane emissions from 2015 to 2016. One possible explanation of this finding is the temporary reduction in the Amazon atmospheric observational network during this period. However, the same decrease is also present in the ST_{-ALL} sensitivity experiment, in which all Amazonian observations are excluded from the inversion. This indicates that the reduction is not driven by the Amazon regional observational network.

3.5 Comparison to other global inversion systems

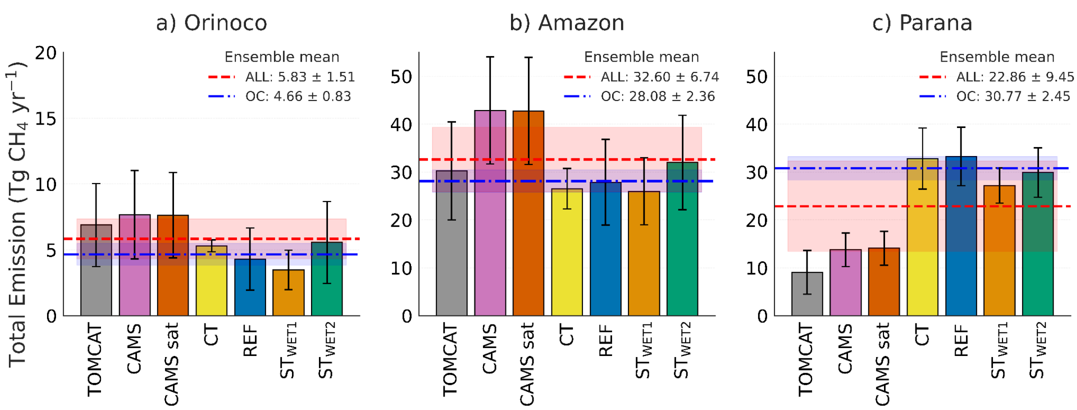

Figure 6. Total methane budget estimated using different global inversion systems across the three South American river basins a) Orinoco, b) Amazon, c) Paraná for the period 2010–2019. The ensemble OC is the ensemble mean of the inversion systems that include in-situ observational constraints (OC) from the Amazon Basin (e.g. CarbonTracker, CarboScope). Error bars represent the IAV calculated as the standard deviation of annual means across years.

A comparison of multiple inversion systems shows a clear difference in total methane emission estimated across the three river basins. The Amazon is the largest regional contributor of methane emissions in all inversion systems, with an ensemble mean estimate of 32.60 ± 6.74 Tg CH_4 yr^{-1} from different inversion systems (Fig. 6). When we focus on inversion systems with observational constraints from the Amazon (CarbonTracker and CarboScope), the ensemble emission (ensemble OC) decreases to 28.0 ± 2.36 Tg CH_4 yr^{-1}, corresponding to a reduction of ~65% in ensemble spread (standard deviation across different inversion system). This indicates that inversion systems without in-situ observational constraints in the region (such as TOMCAT and both CAMS versions) contribute significantly to the overall inter-model spread and may bias the ensemble mean high. It also shows that CarboScope-derived methane flux estimates are consistent with other observationally constrained inversion systems, like CarbonTracker-CH_4 and well within the ensemble range.
The mean methane emission from Orinoco basin across all inversion systems is estimated at 5.83 ± 1.51 Tg CH_4 yr^{-1}. When we only consider the inversion systems which have regional in-situ observational constraints from Amazon basin (CarbonTracker, CarboScope versions), the ensemble mean is reduced to 4.66 ± 0.83 Tg CH_4 yr^{-1}, corresponding to ~45% reduction in the ensemble spread. This reduced spread should not be interpreted as evidence that methane emissions from the Orinoco basin are better constrained by observations. Rather, it reflects the consistent behaviour of the CarbonTracker and CarboScope inversion systems, which assimilate a regional Amazon in-situ observations and therefore produce more similar methane emission estimates for the Orinoco basin.

Finally, the Paraná basin shows the largest ensemble spread across the different inversion systems. The methane emission estimates in the basin show an ensemble mean of 22.86 ± 9.45 Tg CH_4 yr^{-1}, indicating a much larger model spread compared to the other two basins. The inversion estimates separate into two distinct groups: TOMCAT and CAMS estimate emissions below ~15 Tg CH_4 yr^{-1}, whereas CarbonTracker and CarboScope estimate substantially higher emissions, mostly between ~27 and 34 Tg CH_4 yr^{-1}. This corresponds to differences of approximately a factor of two to three between inversion systems. When we only consider the inversion systems with in-situ data from the Amazon, the ensemble mean increased to 30.77 ± 2.45 Tg CH_4 yr^{-1}, reducing the spread by ~74%. Again, there is good agreement among inversions which have in-situ constraints in the Amazon, supporting the redistribution of fluxes

https://doi.org/10.5194/egusphere-2026-5245
Preprint. Discussion started: 28 September 2026

between the Amazon and Paraná basins. This indicates that these observationally constrained inversion systems are more consistent with one another for the Paraná basin.

Overall, the comparison highlights two main findings. First, inversion systems assimilating regional Amazon in-situ observations (CarbonTracker and the CarboScope experiments) produce much more consistent methane emission estimates than the full ensemble, particularly for the Amazon basin where these observations directly constrain the methane fluxes. For the Orinoco and Paraná basins, however, the smaller spread among these inversion systems should not be interpreted as evidence that methane emissions are better constrained by observations, but rather that CarbonTracker and CarboScope produce more consistent emission estimates. This is further illustrated by the contrasting behaviour of the Amazon and Paraná basins across the inversion systems: TOMCAT and both CAMS inversions estimate higher methane emissions for the Amazon and lower emissions for the Paraná basin, whereas CarbonTracker and the CarboScope experiments show the opposite. This indicates that inversion systems assimilating regional Amazon in-situ observations produce consistent methane emission estimates across the South American river basins. Second, the CAMS (surface) and CAMS (satellite+surface) inversion produce nearly identical methane emission estimates for all three basins, indicating that the inclusion of satellite observations has only a limited influence on the basin-integrated methane budgets within the CAMS inversion framework.

3.5.1 Validation of inversion models with independent observations:

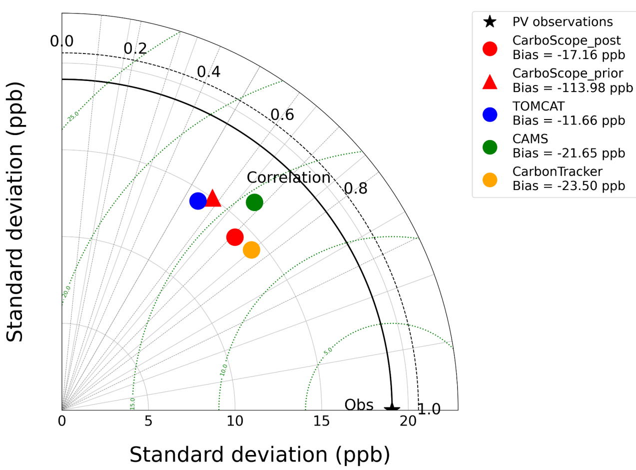

https://doi.org/10.5194/egusphere-2026-5245
Preprint. Discussion started: 28 September 2026

Figure 7. Taylor diagram evaluating the performance of the methane inversion systems against FTIR total-column CH_4 observations at Porto Velho (PV). The diagram compares the posterior CarboScope (REF), prior CarboScope (REF), CarbonTracker, TOMCAT, and CAMS inversion systems.

The inversion systems were evaluated against independent aircraft (MAN and PAN), tower (ATTO), and FTIR (Porto Velho) observations; the more detailed evaluation results are presented Appendix C. The PV site evaluation (Fig 7) shows that all posterior inversion systems underestimate the observed total-column methane, resulting in negative mean biases. However, the magnitude of this bias varies among the inversion systems, with TOMCAT exhibiting the smallest mean bias (mean bias = -11.66 ppb, r =0.54, $p<0.05$), while CarbonTracker (mean bias = -23.50 ppb, r =0.76, $p<0.05$) and the CarboScope posterior (mean bias = -17.16 ppb, r =0.70, $p<0.05$) show the highest correlations with the FTIR observations. The substantial reduction in the CarboScope bias, from approximately −113.98 ppb (r = 0.57, $p<0.05$) in the prior simulation to −17.16 ppb (r =0.70, $p<0.05$) in the posterior, further demonstrates the significant improvement achieved through the assimilation of atmospheric observations in CarboScope inversion system. For the aircraft observations, the largest differences between model and observations occur within the boundary layer (<2 km, -52.23 to 44.77 ppb), where methane concentrations are more strongly influenced by surface emissions, whereas all model performance becomes more comparable in the free troposphere (>2 km), with lower mean bias (-11.59 to 24.55 ppb). Across both atmospheric levels, TOMCAT generally overestimates (Fig C1) the observed variability, whereas CAMS tends to underestimate it (Fig C1). Compared to prior (-88 ppb to -114 ppb), CarboScope posterior shows almost negligible (<1.25 ppb) mean bias at both aircraft sites. At the MAN site, CarbonTracker underestimated CH_4 at both altitude levels. All inversion systems perform poorly at the ATTO tower site, exhibiting very weak correlations with the observations ($r < 0.2$), indicating that all inversion systems struggle to reproduce the near-surface methane variability. Among all inversion systems, CarbonTracker shows the lowest mean bias (mean bias = 4.30 ppb) at ATTO, but corresponding correlation is very low (r=0.16). The remaining differences between the model and observations vary among the different evaluation sites and different atmospheric layers, indicating that they are primarily site specific rather than reflecting a systematic overestimation or underestimation of atmospheric methane.

4 Discussion

https://doi.org/10.5194/egusphere-2026-5245
Preprint. Discussion started: 28 September 2026

4.1 Methane budget of the Orinoco, Amazon and Paraná river basins

The CarboScope inversion estimates mean methane emissions of 28.60 ± 5.15 Tg CH_4 yr^{-1} for the Amazon basin during 2010–2019. This estimate is substantially lower than most previous studies, including Neves et al. (2026; 38–50 Tg CH_4 yr^{-1}), Wilson et al. (2021; 41.7–49.3 Tg CH_4 yr^{-1}), Basso et al. (2021; 46.2 ± 10.3 Tg CH_4 yr^{-1}), and Pangala et al. (2017; 42 ± 5.6 Tg CH_4 yr^{-1}). These differences are primarily explained by differences in basin definition, methodology, and observation constraints. Our estimate is in close agreement with the CarbonTracker inversion (26.52 ± 4.23 Tg CH_4 yr^{-1}), which also assimilates Amazon in-situ observations, and with the posterior fluxes of Wilson et al. (2021), which estimate 30.23 ± 10.24 Tg CH_4 yr^{-1} after applying the same native grid, which indicate that CarboScope is not an outlier.

Much of the discrepancy among previous Amazon methane budgets can be attributed to differences in estimated wetland methane emissions, although these studies use different Amazon basin definitions, making direct quantitative comparisons difficult. Our inversion estimates 16.44 ± 2.98 Tg CH_4 yr^{-1}, compared with 33.8 ± 10.7 Tg CH_4 yr^{-1} reported by Basso et al. (2021) and approximately 32 (29–47) Tg CH_4 yr^{-1} from Hancock et al. (2025). Despite starting from substantially larger wetland priors (38.13 ± 2.51 Tg CH_4 yr^{-1}), the inversion reduces wetland emissions by about 50%, indicating that the assimilated atmospheric observations consistently constrain lower posterior wetland emissions. CarbonTracker reduces prior microbial methane emissions by approximately 30%, which includes the wetland emissions, indicating that strong observational constraints consistently act to reduce the prior fluxes. Although our Amazon wetland estimate is considerably lower than that of Hancock et al. (2025), the total South American methane emissions overlap within uncertainties, with Hancock et al. (2025) increasing from a prior of 96 to a posterior of 121 (109–137) Tg CH_4 yr^{-1}, compared with our CarboScope estimate of 109.73 ± 19.91 to 105.46 ± 11.05 Tg CH_4 yr^{-1}. This agreement at the continental scale suggests that the larger discrepancies are primarily associated with the Amazon basin definition.

A more direct comparison can be made with Basso et al. (2021). Although our inversion additionally assimilates observations from ATTO, both studies are constrained by the same regional aircraft observation network. The difference in methane emission becomes much smaller when expressed per unit area. Our total methane emission corresponds to 12.45 ± 4.08

https://doi.org/10.5194/egusphere-2026-5245
Preprint. Discussion started: 28 September 2026

mg CH_4 m^{-2} day^{-1}, compared with 17.4 ± 3.9 mg CH_4 m^{-2} day^{-1} reported by Basso et al. (2021), while our wetland emission estimate (7.50 ± 3.26 mg CH_4 m^{-2} day^{-1}) compares with 12.7 ± 4.3 mg CH_4 m^{-2} day^{-1}. This indicates that much of the discrepancy in basin-integrated methane budgets arises from differences in the spatial domains. In particular, our Amazon basin mask excludes part of the eastern Amazon, whereas Basso et al. (2021) includes this region, where both Basso et al. (2021) and Wilson et al. (2021) observed higher methane emissions. Including this high emission region would therefore increase the basin-integrated methane budget, explaining much of the difference between the studies. To investigate this we calculate the methane budget for the same area for Amazon as used by (Basso et al., 2021), our inversion estimates are 40.90 ± 3.97 Tg CH_4 yr^{-1}, which is much closer to their reported estimate, suggesting that differences in basin definition contribute substantially to the apparent discrepancy.

The differences among previous Amazon methane budgets largely reflect the substantial uncertainties in estimating wetland methane emissions. The large adjustment of wetland emissions from the prior to the posterior inversion (Fig. 2b) highlights that current wetland models remain poorly constrained, reflecting limitations in representing wetland extent, inundation dynamics, and methane biogeochemical processes, as well as the scarcity of independent observational constraints (Melack et al., 2022).

Posterior methane emissions in the Paraná basin are consistently higher than the prior estimates, indicating that atmospheric observations increase regional emissions. Part of this enhancement may reflect spatial redistribution within the inversion associated with atmospheric transport between the Amazon and Paraná basins. Similar behaviour in CarbonTracker suggests that this redistribution is not unique to CarboScope. However, the ST-$_{\mathrm{ALL}}$ experiment still produces enhanced posterior emissions, indicating that Amazonian observational constraints alone cannot explain the increase. Most of the posterior enhancement is attributed to wetlands (Fig. A5), suggesting that prior wetland inventories may underestimate methane emissions in this region. This interpretation is supported by Hancock et al. (2025) and Parker et al. (2018), which also indicate that wetland prior inventories underestimate methane emissions in the Paraná basin. However, with the current observational network, it is not possible to disentangle inversion-driven redistribution from a genuine correction of underestimated prior emissions. The Paraná lacks regional atmospheric observations, and the

https://doi.org/10.5194/egusphere-2026-5245
Preprint. Discussion started: 28 September 2026

global observation network alone reduces posterior uncertainty by only about 25%. Therefore, although the increase in wetland emissions is consistent with previous studies, its magnitude should be interpreted with caution until additional regional observations become available.

Direct comparison with previous studies is difficult because no study has reported methane emissions for the larger Paraná basin considered here, which includes the Paraná and Paraguay floodplains and the Pantanal wetlands. Hancock et al. (2025) provides the closest comparison, combining their wetland methane emission estimates for the Paraná and Pantanal regions yields a total of approximately 3.4–3.6 Tg CH_4 yr^{-1}. This is substantially lower than our wetland estimate of 14.62 ± 8.24 Tg CH_4 yr^{-1}, primarily because our study considers a much larger spatial domain.

For the Orinoco basin, our estimated methane emissions (3.47–5.58 Tg CH_4 yr^{-1}) agree well with the range reported by Amaral et al. (2026) (3.27–5.97 Tg CH_4 yr^{-1}). Similar to the Amazon, regional methane estimates may change once observations from the Orinoco are assimilated in the inversion system. Amaral et al. (2026) estimated that wetlands contribute 40–70% of the total methane budget, consistent with the ~57% contribution in this study.

4.2 Seasonal variability of the methane emission from the South America river basins

The total methane seasonality from the CarboScope inversion (REF) in the Amazon basin shows the dominant peak during the dry season (August), without any secondary peak in the early part of the year (Fig A5, REF). This result contrasts with several previous studies that have suggested a bimodal seasonal cycle in Amazonian methane emissions (Basso et al., 2021; Wilson et al., 2021). When we examine the sensitivity test results for the seasonality (Fig A5), the secondary peak early in the year (March) does emerge in some sensitivity tests, particularly in the experiment adjusting the vertical profile representation (ST_{VPR}), ST_{-ALL}, ST_{-RBA}, and ST_{Only_ATTO}. However, the magnitude of this secondary peak is very small compared to the dry season maximum and it is not found in all experiments. This suggests that the apparent bimodal pattern is not robust and may be sensitive to the choice of observational constraints and the inversion setup. We performed a sensitivity inversion in which the prior wetland emissions were deseasonalized to remove any prescribed seasonal cycle. Despite the absence of seasonality in the prior, the posterior methane emissions still exhibit a clear seasonal cycle (Fig.

https://doi.org/10.5194/egusphere-2026-5245
Preprint. Discussion started: 28 September 2026

A5, ST_{DS}). Notably, this recovered seasonal pattern closely resembles that of the reference (REF) inversion, indicating that the seasonality is primarily constrained by the atmospheric observations rather than the prior.

To investigate this further, we examined the wetland methane emissions separately. Unlike the total methane flux, wetland emissions consistently show a bimodal structure across almost all experiments, with a first peak around March and a second stronger peak during June. This is consistent with a previous study by Basso et al. (2021), who identified the two distinct wetland emission peaks over the Amazon but they found the second peak during the (August-Oct), whereas in our results (REF) the second peak appears earlier, around June (Fig A5, REF). In Basso et al. (2021), the August peak is largely driven by SAN measurements located in the eastern Amazon, which are influenced by the northeastern Amazon region that is not included in our domain. This spatial mismatch may also contribute to the differences in the observed seasonality. Our results show that this wetland driven double peak seasonality is not reflected in the total methane emissions, and the seasonal cycle of total methane is not controlled by the wetland emissions alone, but rather by the combined emissions from all source categories.

During the dry season, biomass burning becomes an important contributor (~15 %), enhancing the August peak (Fig A5, REF). This pattern is consistent with enhanced fire activity during the dry season and agrees with previous studies on seasonal burning in tropical regions (Ribeiro et al., 2018; De Souza Maria et al., 2025). However, the elevated contribution (~27 %) from the “other” category (including termites and geological emissions) is less well supported by independent studies. For instance, Van Asperen et al. (2021) showed that termite methane emissions are largely controlled by internal biological processes and exhibit minimal seasonal variability. Nevertheless, the limited number of studies on Amazonian termite emissions, including Van Asperen et al. (2021), are based on only a few termite species, meaning that tropical ecosystems with much higher termite diversity may still exhibit different emission behaviours. Therefore, a seasonal signal in termite emissions cannot be fully ruled out, although it is more likely that this feature arises from limitations in the inversion framework. Multiple methane source and sink processes exist within a single grid cell of CarboScope, making it difficult to fully separate their individual contributions. As a result, flux adjustments can be erroneously redistributed among source categories during optimization. This is supported by the observed anticorrelation (~0.4) between wetland and “other” emissions from

https://doi.org/10.5194/egusphere-2026-5245
Preprint. Discussion started: 28 September 2026

the inversion, indicating compensating flux adjustments between these categories. So the peak from the "other" category could be real or just an artifact of the inversion system.

There are relatively few studies that explicitly characterize the seasonal cycle of methane emissions in the Paraná Basin. The Pantanal wetland is the dominant biogenic methane source within this region, and thus the seasonal variability in the basin's wetland-driven emissions. Our analysis indicates a bimodal seasonal pattern, with emission peaks occurring at the beginning and toward the end of the year. Notably, the posterior emissions remain largely consistent with the prior seasonal structure, indicating that the inversion preserves the seasonal characteristics represented in the prior (Fig 4c). This seasonal behaviour is broadly consistent with previous satellite-based studies over the Paraná-Pantanal region. Parker et al. (2018), using GOSAT-constrained WetCHARTs prior, reported a pronounced seasonal cycle over the Paraná region, with methane emissions peaking during the wet season at the start of the year. This agrees well with our results, which also show maximum emissions early in the year. In addition, the seasonal analysis by Alvahi & Kirchhoff (2000) in the Pantanal suggests that the maximum methane emissions occur during the wet season from October to April, with lower methane during the dry season (May - Sep), consistent with the dry season minima and elevated wet-season emissions found in our Paraná Basin estimates. Furthermore, Gloor et al. (2021) showed that methane emissions from the Pantanal are strongly linked to hydrological dynamics, with enhanced emissions occurring during the rising water level (Jan -April).

The seasonal variability of methane emissions in the Orinoco Basin is not yet well understood. However, the recent study by Amaral et al. (2026) shows that methane seasonality in this region is strongly linked to inundation patterns, with maximum emissions occurring during the wet season and peaking in July. This seasonal pattern is highly consistent with our results, which also reveal a strong seasonal cycle in methane emission from the Orinoco (Fig 4a). The seasonal cycle remains consistent across all sensitivity experiments using CarboScope (Fig A5), demonstrating that the seasonal pattern is not sensitive to variations in the inversion configuration. Amaral et al. (2026) further suggest that expanding rice cultivation could modify regional methane seasonality, highlighting that current inventories may not fully capture ongoing changes in seasonal emission patterns.

https://doi.org/10.5194/egusphere-2026-5245
Preprint. Discussion started: 28 September 2026

4.3 Methane flux uncertainty and the role of observational constraints

The sensitivity experiments show that, for the Amazon basin, only the experiment removing regional Amazon observations (ST_{-ALL}) produces changes that exceed the posterior uncertainty, whereas all other sensitivity experiments, including changes in wetland priors, atmospheric chemistry, vertical profile representation, and MDM uncertainty, remain within the posterior uncertainty range. This indicates that these modelling choices have only a minor influence on the posterior methane budget from the basin, while the density of regional atmospheric observations provides the dominant constraint on the posterior emissions. Although the posterior Amazon methane budget is relatively insensitive to the choice of wetland prior, this should not be interpreted as evidence that current wetland models are well constrained. As discussed in Section 4.1, the inversion substantially adjusts wetland emissions relative to their prior estimates, highlighting the large uncertainties associated with existing wetland emission models. These uncertainties come from difficulties in representing wetland extent, inundation dynamics, and methane biogeochemical processes in the Amazon (Fleischmann et al., 2022). A different behaviour is found in the Orinoco basin, where posterior methane emissions remain strongly dependent on the assumed wetland prior. Here, uncertainty associated with wetland extent and prior methane emissions leads to substantially larger differences among posterior estimates than changes in atmospheric chemistry or inversion configuration. Although the global atmospheric observation network provides sufficient large-scale information to reproduce the overall seasonal cycle, it does not fully constrain the regional emission magnitude, leaving the inversion partly prior-driven. In contrast, the Paraná basin shows little sensitivity to any of the tested configurations, with all experiments remaining within the posterior uncertainty. This suggests that, for Paraná, the current inversion configuration provides relatively stable methane budgets despite differences in model assumptions. Together, these results highlight that the uncertainty in methane emissions outside the Amazon is primarily controlled by limited regional observational constraints and the quality of prior emissions, emphasizing the need to expand local atmospheric monitoring networks and improve wetland emission inventories.

4.4 Influence of Amazon observations on neighbouring basins

https://doi.org/10.5194/egusphere-2026-5245
Preprint. Discussion started: 28 September 2026

Although Amazon observations are located outside the Orinoco and Paraná basins, they still provide an important regional constraint. Removing the Amazon stations increases uncertainty in the Orinoco basin and produces unrealistic seasonal behaviour, including negative dry season methane fluxes, demonstrating that these observations improve the physical consistency of the inversion. However, they cannot fully compensate for the absence of local observations, as the Orinoco methane budget remains strongly dependent on prior emissions. In contrast, the Paraná basin shows only a weak response to the removal of Amazon observations, indicating a limited influence of the Amazon network on its posterior methane budget. These results demonstrate that regional observations can improve methane flux estimates beyond the basin in which they are assimilated, but they cannot replace local observational constraints. Expanding atmospheric monitoring into data-sparse regions, particularly the Orinoco basin, together with improved prior wetland emission estimates, will therefore be essential for reducing uncertainties in regional methane budgets. Future integration of satellite methane retrievals could further strengthen the spatial constraints provided by the CarboScope inversion.

5 Conclusions

We integrate observations from both Amazon aircraft-based stations and the Amazon Tall Tower Observatory (ATTO) into a global inversion system. This study represents the first comprehensive assessment of methane fluxes across the Amazon, Orinoco, and Paraná basins using a top-down inversion, which helps to improve our understanding of how regional observational networks influence methane budget estimates across South America.

The inclusion of regional observations significantly reduces Amazon basin emissions to 28.60 ± 5.15 Tg CH_4 yr^{-1}, corresponding to ~5% of the global methane budget (Saunois et al., 2025). Further methane emissions are estimated to be 4.44 ± 0.88 Tg CH_4 yr^{-1} for the Orinoco basin and 30.10 ± 3.95 Tg CH_4 yr^{-1} for the Paraná basin. The seasonal cycle of total methane emissions in the Amazon basin shows a single peak driven by combined wetland, fire, and other sources (termites, herbivores (wild ruminants), and geological emissions). In contrast, wetland emissions alone exhibit a bimodal structure, with peaks during the wet season and again in June. The Amazon basin dominates the interannual variability of methane fluxes across

https://doi.org/10.5194/egusphere-2026-5245
Preprint. Discussion started: 28 September 2026

South America in inversion based estimates. Leave-one-out (LOO) experiments show that no single observation site dominates methane flux estimates in the Amazon basin, but the full regional observational network provides strong constraints. ATTO alone plays an important role in constraining methane emissions as well as seasonal cycles, but accurate flux estimates require a dense and well distributed measurement network. The Amazon basin is strongly constrained by regional observations, whereas the Orinoco basin is more sensitive to prior assumptions, and the Paraná basin shows a weak sensitivity to Amazonian observations.

Overall, this study highlights the critical importance of regional in-situ observation networks for improving methane budget estimates across South American basins. While the global observational network provides some constraint, expanding local measurements, particularly in under-constrained regions such as the Orinoco and Paraná basins, is essential for reducing uncertainties and achieving more reliable methane flux estimates. Future work should focus on enhancing observational coverage, and integrating additional observational platforms like satellite measurements while ensuring the long-term maintenance of existing in situ observational networks, to further refine methane flux estimates across South America.

https://doi.org/10.5194/egusphere-2026-5245
Preprint. Discussion started: 28 September 2026

Appendix A

Table A1.Model-data-mismatch uncertainty (MDM) for different station classes in the CarboScope inversion system for the REF case. All station classes are assimilated in the inversion; however, the sensitivity analysis presented in this study focuses on the Continental tall tower and Aircraft station classes.

Description	Model data mismatch σ_{mod} = 35 ppb
Remote (oceanic, e.g., islands, Antarctica)	σ_{mod}
Ocean ship-board	σ_{mod}
At/near shore (ocean-continent boundary)	σ_{mod}*1.5
Continental site (surface)	σ_{mod} *3
Continental mountain site	σ_{mod}*1.5
Continental tall tower*	σ_{mod} *3
Shore with diurnal sea-breeze	σ_{mod}
Mountain with diurnal upslope winds	σ_{mod}
Remote with diurnal upslope winds	σ_{mod}
Urban polluted site	σ_{mod} * 5
Aircraft*	σ_{mod}

(*An asterisk (*) in the Description column indicates the Continental tall tower and Aircraft station classes investigated in the MDM sensitivity experiments of this study.)

https://doi.org/10.5194/egusphere-2026-5245
Preprint. Discussion started: 28 September 2026

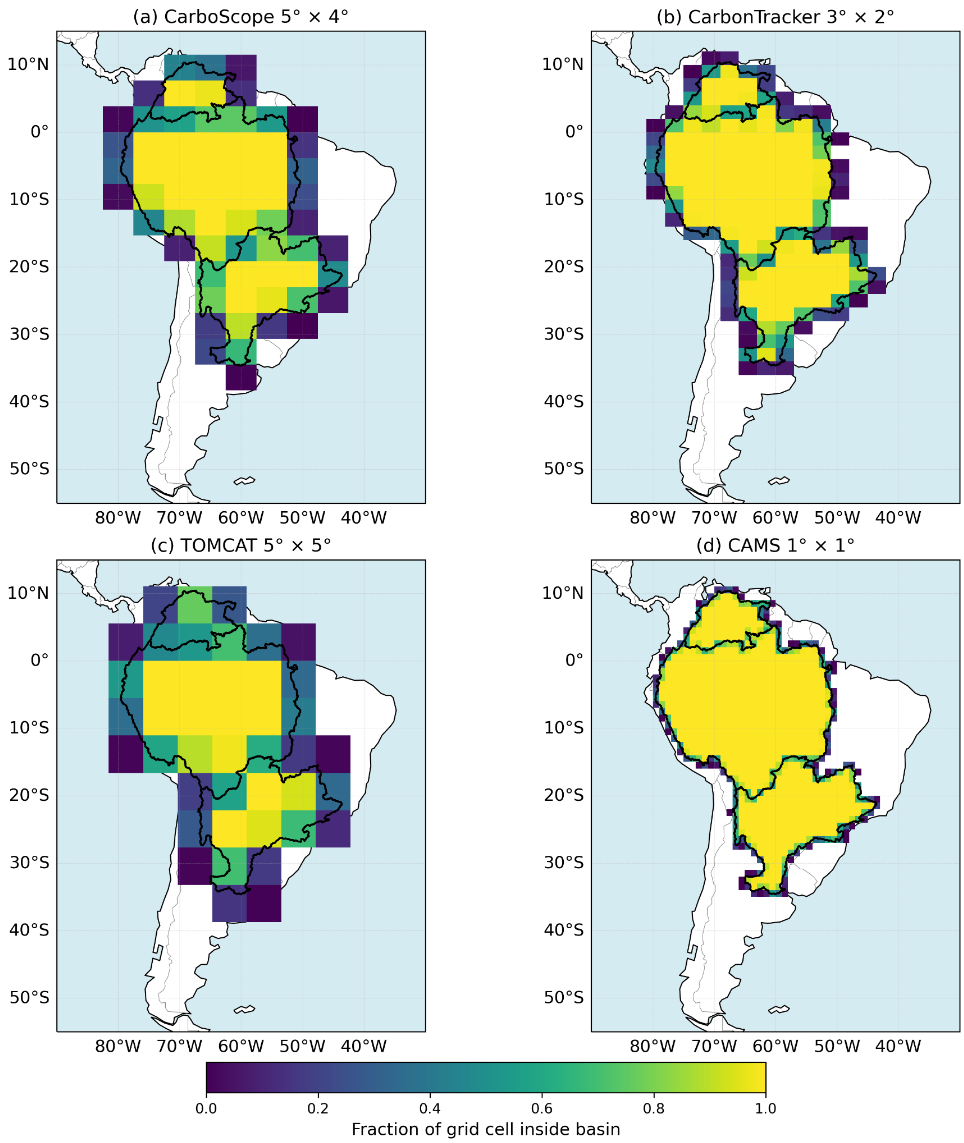

1016

1017 **Figure A1.** Fractional basin masks used for methane flux integration in the four inversion systems: (a)
1018 CarboScope, (b) CarbonTracker , (c) TOMCAT and (d) CAMS . Colors represent the fraction of each model grid
1019 cell contained within the Amazon, Orinoco, and Paraná river basins (0–1). The black polygons show the original
1020 river basin boundaries derived from the HydroBASINS dataset (Lehner and Grill, 2013), which were used to
1021 generate the fractional masks for each model grid.

https://doi.org/10.5194/egusphere-2026-5245
Preprint. Discussion started: 28 September 2026

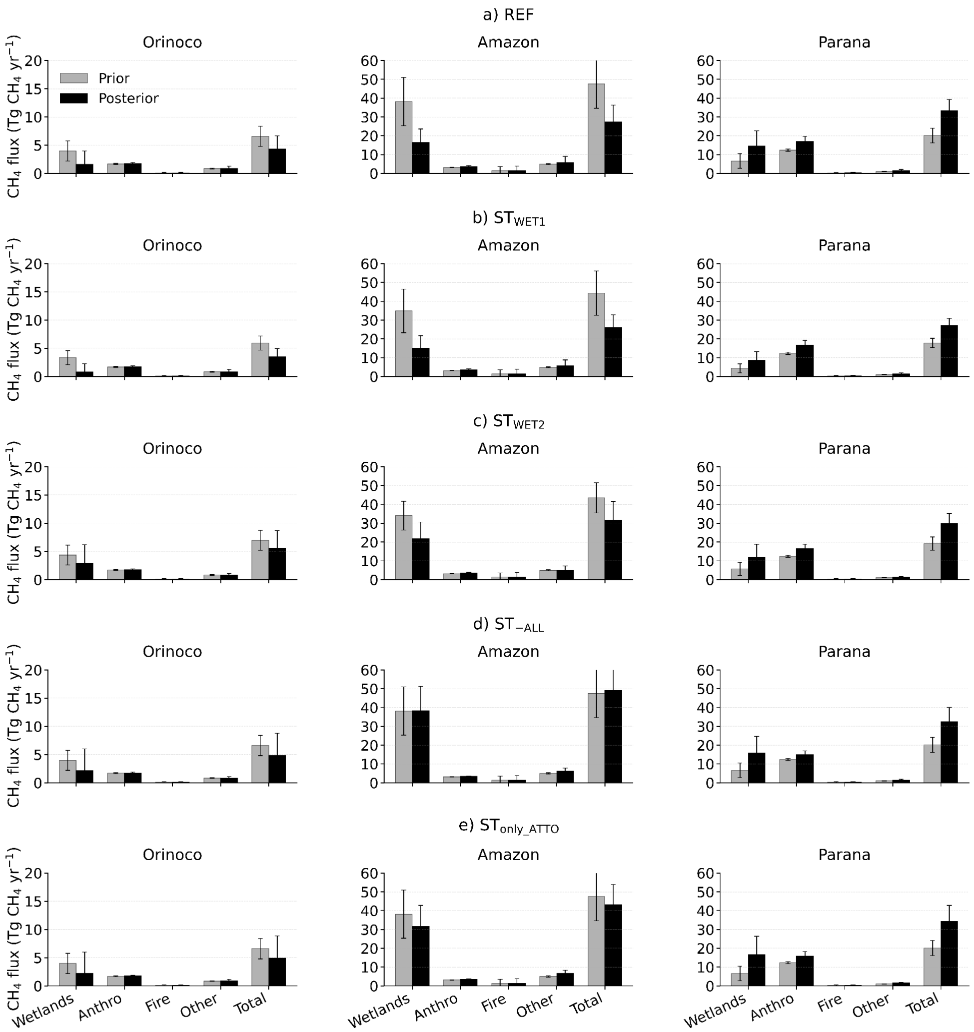

1022

1023 **Figure A2.** Mean prior and posterior methane emissions from different source categories (Wetlands,
1024 Anthropogenic, Fire, Other, and Total) for the Orinoco, Amazon, and Paraná river basins. Results are shown
1025 following experiments (ST$_{WET}$): a) REF, b) ST$_{WET1,}$ c) ST$_{WET2,}$ d) ST$_{-ALL}$, e)ST$_{only_ATTO.}$ The errorbar in the
1026 figure shows the IAV.

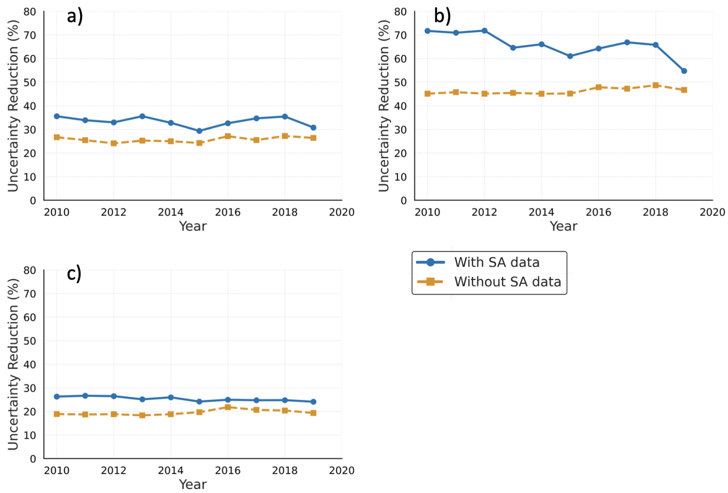

Figure A3. Posterior uncertainty reduction in three South American river basins: (a) Orinoco, (b) Amazon, and (c) Paraná. Results are shown for two inversion configurations: with and without the inclusion of in-situ observations in the Amazon basin.

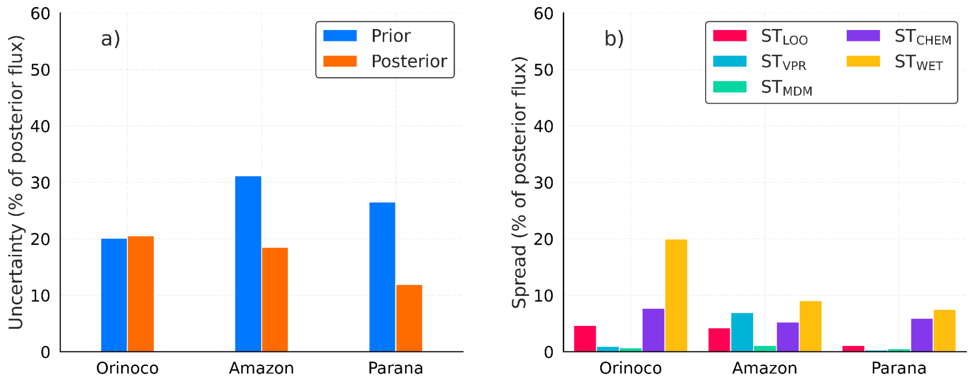

Figure A4. (a) Prior and posterior uncertainty from the inversion system in terms of percentage. b)Variability (%) or relative spread in posterior methane fluxes across sensitivity experiments from the three South American river basins.

https://doi.org/10.5194/egusphere-2026-5245
Preprint. Discussion started: 28 September 2026

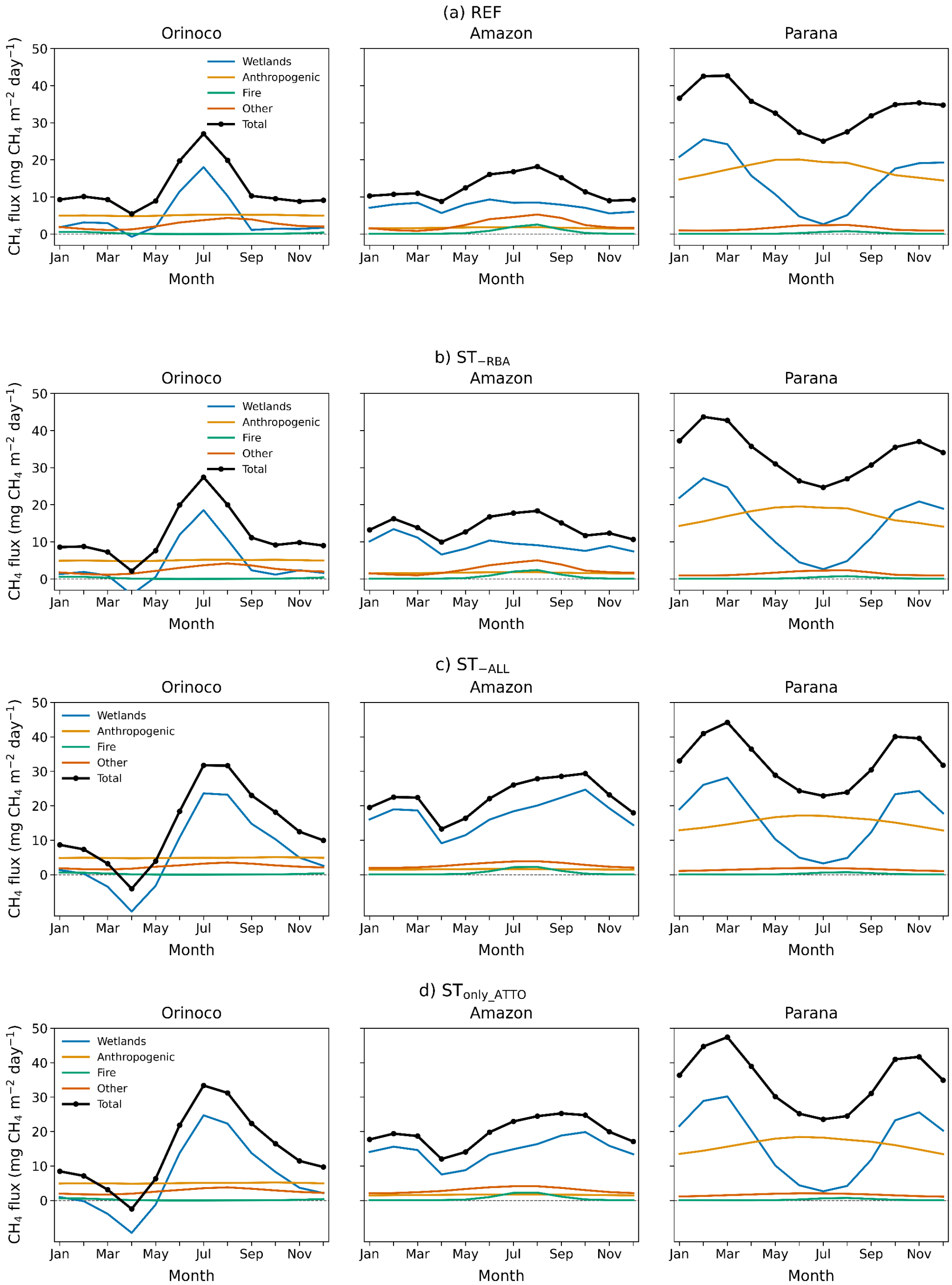

https://doi.org/10.5194/egusphere-2026-5245
Preprint. Discussion started: 28 September 2026

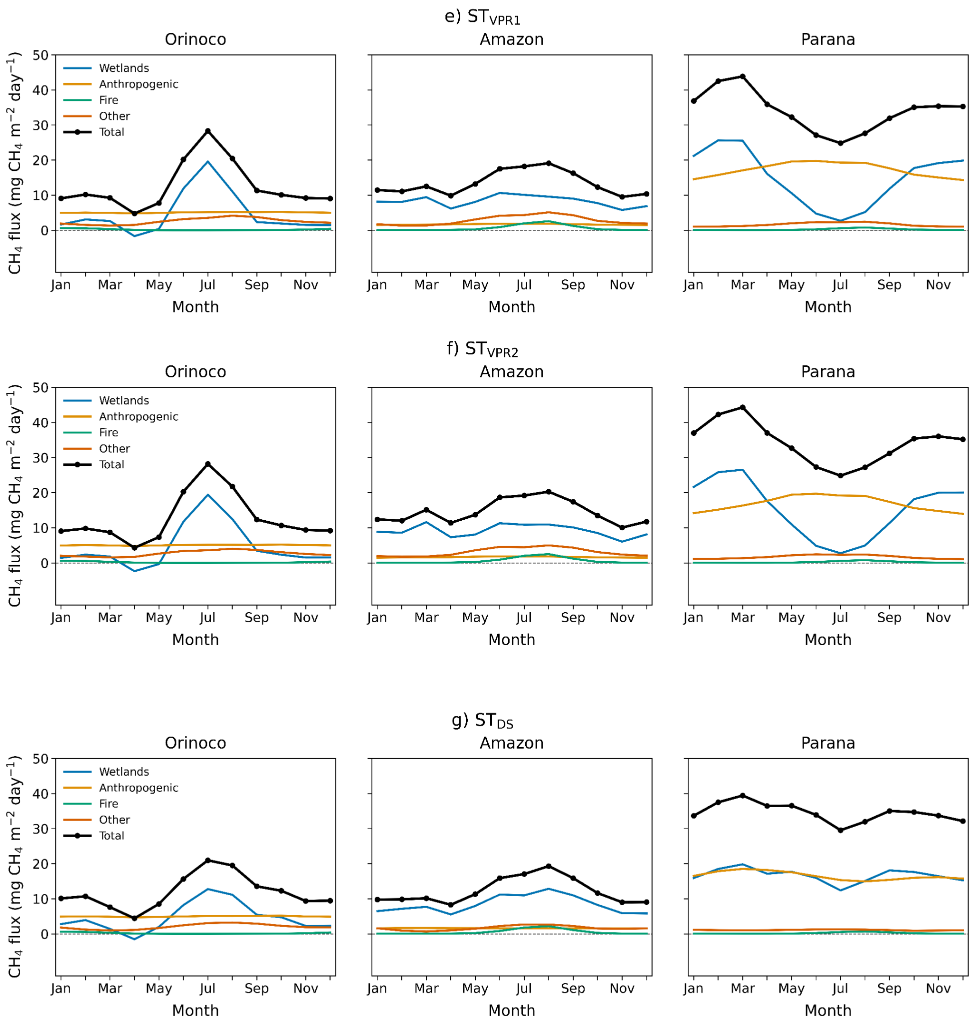

Figure A5. Seasonal cycle of posterior methane fluxes for each emission category across the Amazon, Orinoco, and Paraná basins, as derived from all CarboScope sensitivity experiments a)REF , b)ST_{RBA} , c) ST_{ALL}, d) ST_{only_ATTO}, e) ST_{VPR1}, f)ST_{VPR2}, g)ST_{DS}.

https://doi.org/10.5194/egusphere-2026-5245
Preprint. Discussion started: 28 September 2026

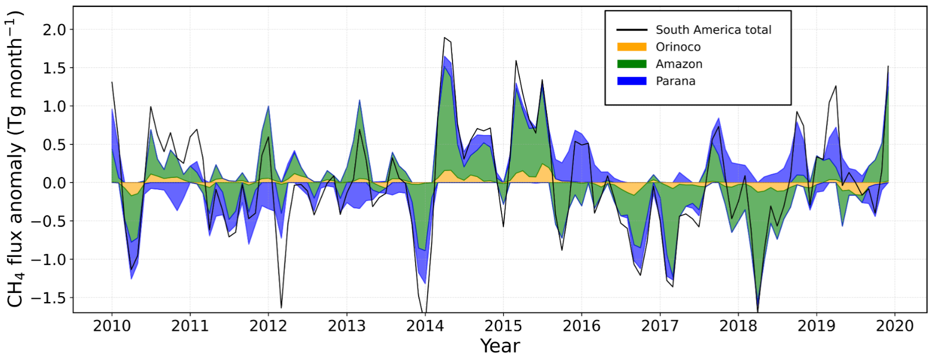

1047

1048 **Figure A6.** Time series of prior and posterior methane emission anomalies from 2010 to 2019 for the study basins
1049 without the regional constraints in the inversion system (ST-ALL).

1050

1051

https://doi.org/10.5194/egusphere-2026-5245
Preprint. Discussion started: 28 September 2026

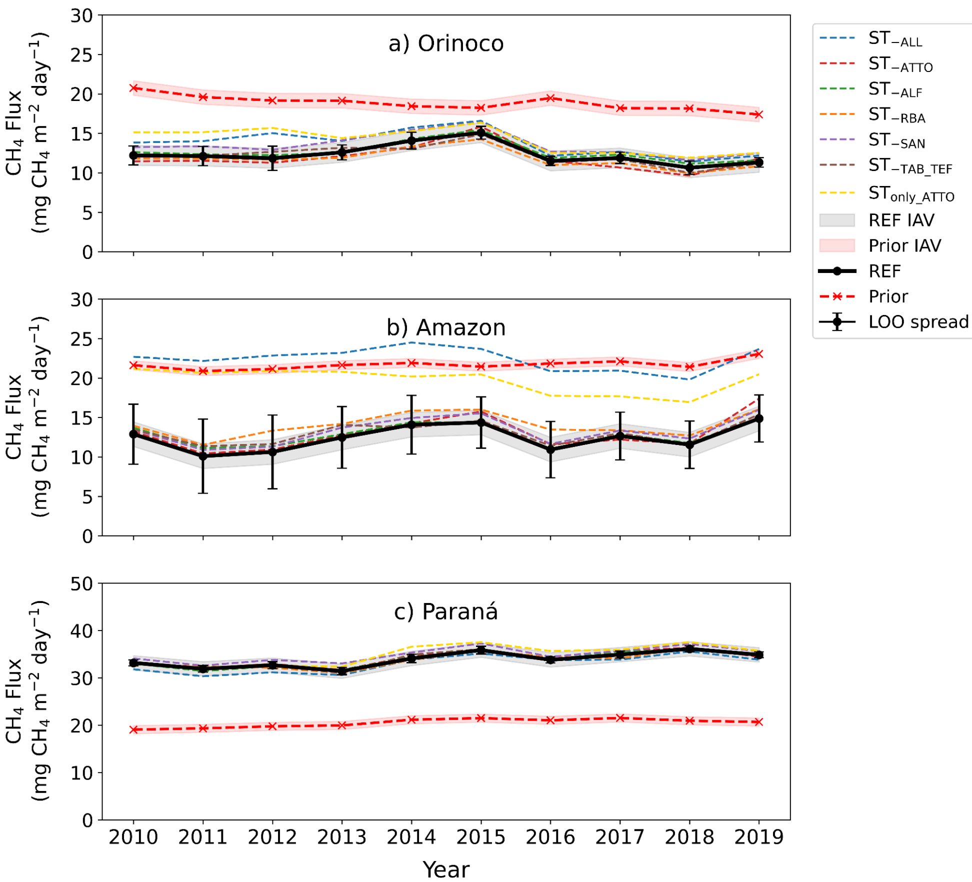

1052

1053 **Figure A7.** Mean Annual total CH_4 fluxes from CarboScope over South America (SA) basins. (a) Orinoco, (b)
1054 Amazon, and (c) Paraná basins. Results are shown for leave-one-out (LOO) experiments (dashed colored lines),
1055 in which individual stations are excluded from the inversion (a "–" indicates the station excluded in a given
1056 experiment), and for an inversion using only ATTO observations (dashed yellow line). These are compared with
1057 the REF inversion including all stations ("All", solid black line), where the shaded envelope represents the
1058 interannual variability (IAV) for each month across all years, and the prior flux estimate (red dashed line).

1059

1060

https://doi.org/10.5194/egusphere-2026-5245
Preprint. Discussion started: 28 September 2026

Appendix B. Description of different atmospheric inversion system

B1 CAMS-CH_4 Inversions

The Copernicus Atmosphere Monitoring Service (CAMS) provides global, inversion-optimized methane flux estimates using atmospheric observations and a variational data assimilation framework version v2022r2. The CAMS CH_4 flux inversions are implemented using the TM5-4DVAR system (Bergamaschi et al., 2013; Copernicus Atmosphere Monitoring Service, 2020; Segers and Nanni 2023) and are available in two versions based on the type of observational data assimilated.

CAMS (surface) assimilates in-situ observations only. These consist of dry-air mole fraction measurements from the NOAA global surface observation network, which provides long-term, high-precision methane measurements from monitoring stations worldwide.

CAMS (satellite + surface), incorporates satellite observations in addition to in-situ measurements for flux optimization. In this version, total column methane retrievals from the Greenhouse Gases Observing Satellite (GOSAT) are assimilated together with surface observations, allowing for enhanced spatial coverage, particularly over regions with sparse in-situ measurements.

Both CAMS inversion versions use the same prior flux inventories and atmospheric transport model. Details of the prior flux components and the atmospheric transport model are summarized in Table 3. To represent uncertainties in the prior emissions, source-specific uncertainty values are prescribed: wetlands, rice cultivation, and biomass burning are assigned uncertainties of 100%, while other anthropogenic sources are assigned an uncertainty of 50%. Spatial error correlations are imposed with a length scale of 500 km. No temporal correlation is applied to wetlands, rice, and biomass burning emissions in order to allow for strong seasonal variability, whereas anthropogenic emissions are assigned an exponential temporal correlation with a decay timescale of 9.5 months.

https://doi.org/10.5194/egusphere-2026-5245
Preprint. Discussion started: 28 September 2026

Further details on the CAMS methane inversion framework can be found in Segers and Nanni. (2023).

B2 CarbonTracker-CH_4 -2023 (CT-CH4-2023)

CarbonTracker provides global methane flux estimates from microbial, pyrogenic, and fossil sources. The microbial category includes both natural emissions (e.g., wetlands, termites, and other aquatic sources) and anthropogenic sources (e.g., waste, rice cultivation, and ruminants). It is implemented with the TM5-4DVAR framework. The inversion uses both observed atmospheric methane concentrations and stable carbon isotopic ratios ($\delta^{13}C$-CH_4). CarbonTracker assimilates observed atmospheric methane concentration from the Amazon basin.

For methane mole fraction measurements, CarbonTracker assimilates data from NOAA Global Monitoring Laboratory (GML) GLOBALVIEWplus (GV+) products, which are constructed using the Observation Package (ObsPack) framework (citation needed). Isotopic ($\delta^{13}C$–CH_4) measurements are compiled from the Institute for Arctic and Alpine Research (INSTAAR) and additional isotope laboratories, as described in Oh et al. (2023).

Details of the prior emissions and atmospheric transport model are summarized in Table 3. The prior emission uncertainties are set to 120% for microbial sources, 150% for fossil sources, and 100% for pyrogenic sources. Off-diagonal spatial error correlation lengths are 500 km for microbial emissions, 700 km for fossil emissions, and 300 km for pyrogenic emissions. The corresponding off-diagonal temporal correlation lengths are 2 months for microbial sources, 6 months for fossil sources, and 1 month for pyrogenic sources. For more details please refer to Oh et al. (2023).

B3 TOMCAT

TOMCAT is a 3D global atmospheric chemistry and transport model (Chipperfield, 2006). In the study by Wilson et al. (2021), TOMCAT was combined with the INVICAT inversion framework to produce posterior CH_4 fluxes. It optimizes posterior fluxes in two categories: "Fossil" and "Agriculture and Natural". It assimilated column-averaged dry-air mole fraction methane retrievals (XCH_4) v7.2 from the University of Leicester GOSAT (Greenhouse Gases Observing Satellite) product (Parker et al., 2020) and flask observation from global long-term surface data of methane provided by NOAA GML. This surface flask dataset includes 56 background monitoring sites where air samples are collected weekly to biweekly.

Remaining details about the prior emissions are provided in Table 3. Prior emission uncertainty is set at 250% for all categories. The spatial correlation length is 500 km for all categories and no temporal correlation is applied to natural, agricultural, and biomass burning emissions in order to allow for strong seasonal variability, whereas anthropogenic emissions are assigned an exponential temporal correlation with a decay timescale of 9.5 months. For more detail about the inversion setup please refer to Chipperfield (2006) and Wilson et al. (2021).

Appendix C. Detailed evaluation of the inversion systems

This appendix presents a detailed evaluation of the inversion systems against the independent aircraft (MAN and PAN), tower (ATTO), and FTIR (Porto Velho) observations. The corresponding Taylor diagrams are shown in Fig. C1

https://doi.org/10.5194/egusphere-2026-5245
Preprint. Discussion started: 28 September 2026

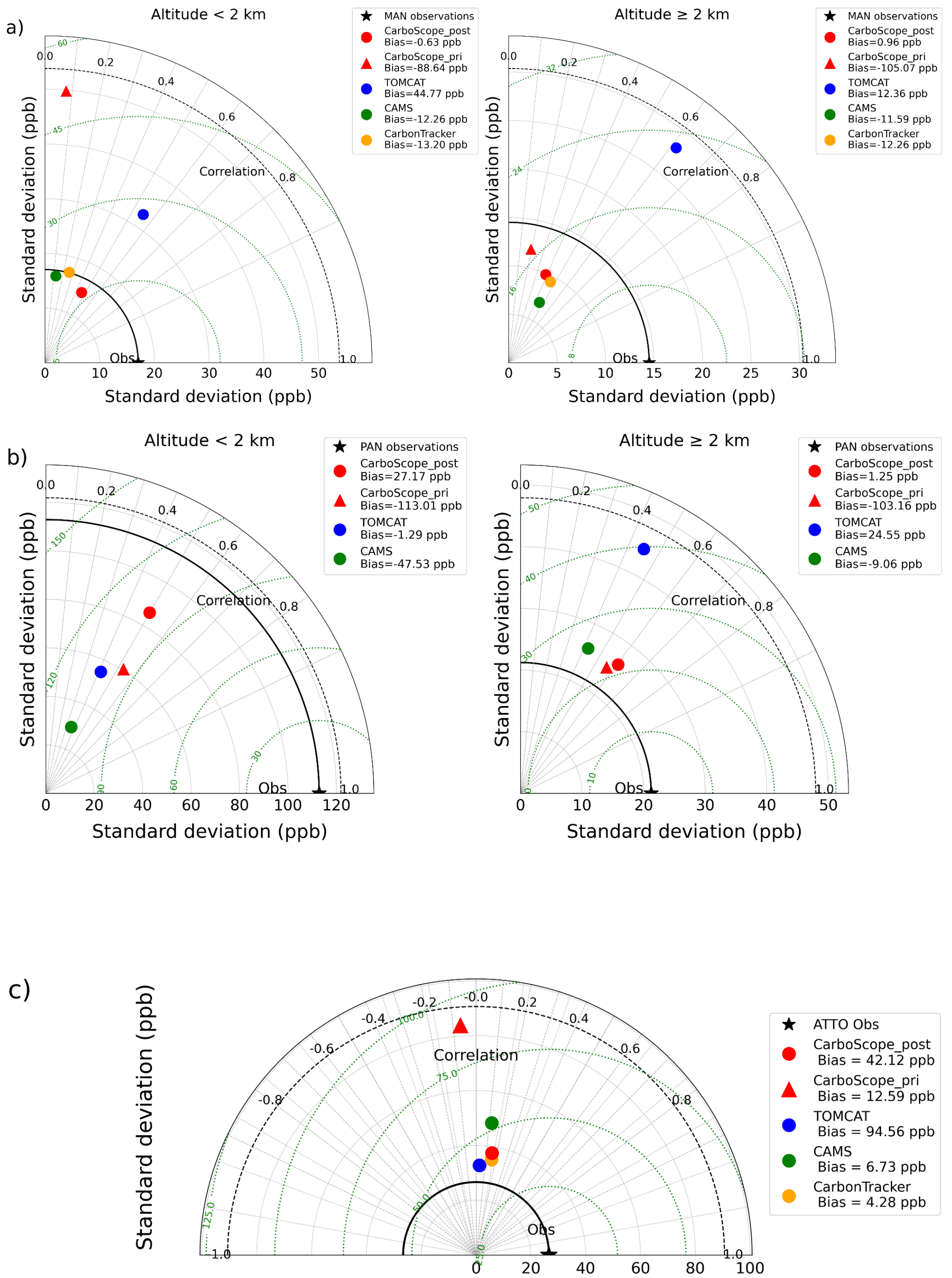

Figure C1. Taylor diagrams evaluating the performance of the methane inversion systems against independent atmospheric observations. Panels (a) and (b) show comparisons with aircraft measurements over Manaus and

https://doi.org/10.5194/egusphere-2026-5245
Preprint. Discussion started: 28 September 2026

Pantanal, respectively, separated into the boundary layer (<2 km) and free troposphere (>2 km). Panel (c) shows the comparison with continuous methane observations at the ATTO tower. The posterior CarboScope (REF), CarbonTracker, TOMCAT, and CAMS inversion systems are compared.

For the MAN aircraft observations, the CarboScope posterior reproduces the surface methane concentrations (<2 km) with an almost negligible mean bias (-0.63 ppb), the lowest RMSE (16.5 ppb), and a model standard deviation (14.5 ppb) that is close to the observed variability (17.0 ppb). This represents a clear improvement over the CarboScope prior, which strongly underestimates methane concentrations (mean bias = −88.6 ppb), overestimates their variability (49.8 ppb), and shows almost no correlation with the observations (r = 0.08). Although TOMCAT exhibits the highest correlation (r = 0.55), it substantially overestimates both methane concentrations (mean bias = 44.8 ppb) and atmospheric variability (32.5 ppb compared to an observed standard deviation of 17.0 ppb), resulting in the largest RMSE (52.4 ppb). CAMS and CarbonTracker reproduce the magnitude of the observed variability reasonably well, with standard deviations of 16.0 and 17.1 ppb, respectively, but both underestimates mean methane concentrations. CarbonTracker shows a higher correlation than CAMS (r = 0.26 compared with 0.12), although both have similar RMSE values of ~ 25 ppb.

In the free troposphere (>2 km), the CarboScope posterior again provides the best overall agreement, combining an almost negligible mean bias (0.96 ppb) with the lowest RMSE (14.1 ppb), although it underestimates the observed variability (9.9 compared with 14.5 ppb). In contrast, the CarboScope prior has a large negative mean bias (−105.1 ppb) and a weak correlation (r = 0.19), demonstrating the strong improvement achieved by the inversion. TOMCAT again shows the highest correlation (r = 0.61), but continues to overestimate both methane concentrations and variability. CAMS and CarbonTracker show similar performance, with moderate correlations (r = 0.45 and 0.46, respectively) and negative mean biases of approximately −12 ppb. Both underestimate the observed variability, with model standard deviations of 7.0 ppb for CAMS and 9.4 ppb for CarbonTracker, and RMSE values of 17.4 and 18.0 ppb, respectively.

The PAN aircraft observations show a similar overall behaviour. In the near surface (< 2km), the CarboScope prior exhibits the highest correlation (r = 0.53) but considerably underestimates CH_4, with a mean bias of −113.0 ppb and the highest RMSE (148.0 ppb). The CarboScope posterior improves the agreement, reducing the bias to +27.2 ppb and the RMSE to 105.7 ppb,

https://doi.org/10.5194/egusphere-2026-5245
Preprint. Discussion started: 28 September 2026

while maintaining a moderate correlation (r = 0.50) and reproducing the observed variability more closely (86.0 ppb compared with 112.8 ppb observed). TOMCAT has the smallest absolute mean bias (-5.3 ppb), it substantially underestimates the observed variability (55.1 ppb), resulting in an RMSE comparable to that of CarboScope. CAMS performs least well, exhibiting both the largest negative mean bias (-52.2 ppb) and the smallest variability (29.5 ppb), indicating a pronounced underestimation of the observed atmospheric variability.

Above 2 km, the CarboScope posterior again provides the best overall agreement with the observations, combining the highest correlation (r = 0.61), an almost negligible mean bias (1.25 ppb), Although the CarboScope prior reproduces the observed variability and temporal pattern reasonably well (r=0.56), it has a large negative bias (−103.2 ppb), resulting in a high RMSE (105.4 ppb). TOMCAT considerably overestimates both methane concentrations and variability, whereas CAMS maintains moderate negative biases while reproducing the observed variability more realistically than TOMCAT.

The evaluation against the ATTO tower observations indicates that reproducing near-surface methane variability at this site remains challenging for all inversion systems. All models exhibit very weak correlations (r < 0.2), indicating that none adequately reproduces the observed temporal variability. Although the CarboScope prior has a relatively small mean bias (+12.6 ppb), it shows a weak negative correlation (r= −0.07), excessive variability, and a high RMSE (90.6 ppb). The CarboScope posterior reduces the RMSE to 59.9 ppb and brings the variability closer to the observations, but increases the positive bias to 42.1 ppb. CarbonTracker exhibits the smallest mean bias (4.3 ppb) and the lowest RMSE (40.9 ppb), although its correlation remains similarly weak (r = 0.16). TOMCAT performs the poorest, showing both the largest positive bias (94.6 ppb) and the highest RMSE (103.2 ppb), whereas CAMS exhibits only a small positive bias (6.7 ppb) but considerably overestimates the observed variability.

The PV evaluation compares the model and observed total column methane mole fractions (xCH_4). xCH_4 was calculated as the ratio of the retrieved total CH_4 column to the total dry-air column (or an equivalent dry-air proxy), resulting in the column-averaged dry-air mole fraction of methane (Flood et al., 2024). All posterior inversion systems exhibit negative mean biases, indicating a systematic underestimation of the observed methane column at this site. Among the posterior inversions, TOMCAT shows the smallest mean bias (−11.7 ppb), whereas

https://doi.org/10.5194/egusphere-2026-5245
Preprint. Discussion started: 28 September 2026

CarbonTracker exhibits the highest correlation with the observations (r = 0.76), closely followed by the CarboScope posterior (r = 0.71). Although CarbonTracker has the highest correlation, its mean bias (−23.5 ppb) is larger than that of both TOMCAT and the CarboScope posterior (−17.2 ppb). The CarboScope posterior also reduces the mean bias substantially compared with the prior simulation (from −113.98 ppb to −17.16 ppb), indicating a considerable improvement in the simulated methane column following the inversion. The systematic negative bias observed across all posterior inversion systems at PV sites. The Taylor diagram further indicates that the CarboScope posterior reproduces the observed variability better than the prior simulation, although its standard deviation (~10 ppb) remains considerably lower than the observed standard deviation (~18.5 ppb). Similar underestimation of variability is found for the other posterior inversion systems, suggesting that they capture the temporal evolution of methane but damp the magnitude of the observed fluctuations.

Code and data availability.

The posterior methane fluxes from the REF, STWET, and STWET2 inversion experiments and Fractional basin mask used for the CarboScope are available from the Edmond Research Data Repository at,

https://edmond.mpg.de/dataset.xhtml?persistentId=doi:10.17617/3.YH7RYS

The atmospheric CH_4 observations used in the inversions are available from several public repositories. The NOAA GML ObsPack v6.0 dataset is available at https://doi.org/10.25925/20231001. Data from the ICOS Carbon Portal are available at https://doi.org/10.18160/KDMT-V6CG (ICOS RI et al., 2024), and observations from the World Data Centre for Greenhouse Gases (WDCGG) are available at https://doi.org/10.50849/WDCGG_CH4_ALL_2023.

The Amazon aircraft vertical-profile measurements are available from PANGAEA at https://doi.org/10.1594/PANGAEA.926834 (Gatti et al., 2021). The ATTO CH_4 measurements used in this study can be requested through the ATTO Data Portal (https://www.attodata.org/). CH_4 measurements from the Pantanal aircraft campaign are available from the CEDA archive at http://catalogue.ceda.ac.uk/uuid/d309a5ab60b04b6c82eca6d006350ae6, and the Manaus

https://doi.org/10.5194/egusphere-2026-5245
Preprint. Discussion started: 28 September 2026

aircraft CH_4 measurements are available at http://dx.doi.org/10.25925/20230922. The FTIR observations used for independent evaluation are available upon request from the respective data provider.

The river-basin masks used in this study were obtained from the HydroBASINS dataset and are available at https://www.hydrosheds.org/products/hydrobasins

Author contributions.

SW and SB were responsible for the conceptualization of the study and the development of the methodology. SW conducted all inversion experiments, curated and formally analyzed the data, performed the inversion intercomparison, interpreted the results, prepared the visualizations, and wrote the original draft. SB supervised the research project and reviewed and edited the manuscript. LSB contributed to the methodology and software through technical support for the inversion setup, assisted with the interpretation of the results, and reviewed and edited the manuscript. CR developed the CarboScope inversion system and contributed to the methodology, software, and technical implementation of the inversion experiments. ASF, JFA, JM, SH, and JM (Julia) reviewed and edited the manuscript. JL and DW operated the ATTO measurement system until 2021 and provided the ATTO observational data. YO and LB provided the CarbonTracker posterior flux data used for the inversion intercomparison, and YO additionally reviewed the manuscript. CV provided the Porto Velho observational data used for the inversion evaluation and reviewed the manuscript. JBM conducted the Manaus aircraft measurements. CW provided the TOMCAT simulated mole fractions and posterior flux data used for the inversion intercomparison and reviewed and edited the manuscript. All authors contributed to the discussion of the results and approved the final manuscript.

Competing interests.

At least one of the co-authors is a member of the editorial board of Atmospheric Chemistry and Physics.

Acknowledgements.

We acknowledge the Instituto Nacional de Pesquisas da Amazonia as well as the Amazon State University (UEA), FAPEAM, LBA/INPA and SDS/CEUC/RDS-Uatumã for continuous support and logistical management. We express our gratitude to the data providers of the global monitoring network and specifically the LaGEE/INPE team coordinated by Luciana Gatti (Aircraft vertical profiles), the PI of the INPE aircraft network. The FTIR installation and measurements at Porto Velho were funded by the Belgian Science Policy Office (BELSPO). We gratefully acknowledge Filip De Smet, Nicolas Kumps, Bavo Langerock, Martine De Mazière (BIRA-IASB), and Carlos Bauer Aquino (IFRO) for their essential contributions to the data acquisition.

Financial support.

The ATTO project has been funded by the German Federal Ministry of Education and Research (BMBF, contracts 01LB1001A and 01LK1602A) and the Brazilian Ministério da Ciencia, Tecnologia e Inovação (MCTI/FINEP contract 01.11.01248.00) and the Max Planck Society. SW was funded by the German Academic Exchange Service (DAAD) and the International Max Planck Research School on global biogeochemical cycles. SB was funded by the Max Planck Society. Chris Wilson is funded via the UK National Centre for Earth Observation (NE/R016518/1 and NE/N018079/1) and the EU-funded IM4CA project (doi:10.3030/101183460). The article processing charges for this open-access publication were covered by the Max Planck Society.

https://doi.org/10.5194/egusphere-2026-5245
Preprint. Discussion started: 28 September 2026

References

Alsdorf, D. E., Melack, J. M., Dunne, T., Mertes, L. A. K., Hess, L. L., and Smithß, L. C.: Interferometric radar measurements of water level changes on the Amazon Øood plain, 2000.

Amaral, J. H. F., Botía, S., Quintero, P. T., Gutierrez, A. S., David Ho, Sanchez, A., Avila-Diaz, A., Uhde, A., Quesada, B., Winton, R. S., Sierra, C. A., Navarro-Ramírez, M. A., Pardo, D. D., and Hantson, S.: Methane fluxes from tropical wetlands of the Orinoco River Basin and their regional implications, 2026.

Andreae, M. O., Acevedo, O. C., Araùjo, A., Artaxo, P., Barbosa, C. G. G., Barbosa, H. M. J., Brito, J., Carbone, S., Chi, X., Cintra, B. B. L., Da Silva, N. F., Dias, N. L., Dias-Júnior, C. Q., Ditas, F., Ditz, R., Godoi, A. F. L., Godoi, R. H. M., Heimann, M., Hoffmann, T., Kesselmeier, J., Könemann, T., Krüger, M. L., Lavric, J. V., Manzi, A. O., Lopes, A. P., Martins, D. L., Mikhailov, E. F., Moran-Zuloaga, D., Nelson, B. W., Nölscher, A. C., Santos Nogueira, D., Piedade, M. T. F., Pöhlker, C., Pöschl, U., Quesada, C. A., Rizzo, L. V., Ro, C.-U., Ruckteschler, N., Sá, L. D. A., De Oliveira Sá, M., Sales, C. B., Dos Santos, R. M. N., Saturno, J., Schöngart, J., Sörgel, M., De Souza, C. M., De Souza, R. A. F., Su, H., Targhetta, N., Tóta, J., Trebs, I., Trumbore, S., Van Eijck, A., Walter, D., Wang, Z., Weber, B., Williams, J., Winderlich, J., Wittmann, F., Wolff, S., and Yáñez-Serrano, A. M.: The Amazon Tall Tower Observatory (ATTO): overview of pilot measurements on ecosystem ecology, meteorology, trace gases, and aerosols, Atmos. Chem. Phys., 15, 10723–10776, https://doi.org/10.5194/acp-15-10723-2015, 2015.

Barbosa, P. M., Melack, J. M., Amaral, J. H. F., MacIntyre, S., Kasper, D., Cortés, A., Farjalla, V. F., and Forsberg, B. R.: Dissolved methane concentrations and fluxes to the atmosphere from a tropical floodplain lake, Biogeochemistry, 148, 129–151, https://doi.org/10.1007/s10533-020-00650-1, 2020.

Basso, L. S., Marani, L., Gatti, L. V., Miller, J. B., Gloor, M., Melack, J., Cassol, H. L. G., Tejada, G., Domingues, L. G., Arai, E., Sanchez, A. H., Corrêa, S. M., Anderson, L., Aragão, L. E. O. C., Correia, C. S. C., Crispim, S. P., and Neves, R. A. L.: Amazon methane budget derived from multi-year airborne observations highlights regional variations in emissions, Commun. Earth Environ., 2, 246, https://doi.org/10.1038/s43247-021-00314-4, 2021.

Basso, L. S., Rödenbeck, C., Brovkin, V., Georgievski, G., Heimann, M., and Göckede, M.: Quantifying Arctic-boreal methane emissions using atmospheric observations and a global inverse model, Npj Clim. Atmos. Sci., 9, 80, https://doi.org/10.1038/s41612-026-01348-1, 2026.

Basu, S., Lan, X., Dlugokencky, E., Michel, S., Schwietzke, S., Miller, J. B., Bruhwiler, L., Oh, Y., Tans, P. P., Apadula, F., Gatti, L. V., Jordan, A., Necki, J., Sasakawa, M., Morimoto, S., Di Iorio, T., Lee, H., Arduini, J., and Manca, G.: Estimating emissions of methane consistent with atmospheric measurements of methane and δ^{13} C of methane, Atmos. Chem. Phys., 22, 15351–15377, https://doi.org/10.5194/acp-22-15351-2022, 2022.

https://doi.org/10.5194/egusphere-2026-5245
Preprint. Discussion started: 28 September 2026

Belikov, D. A., Patra, P. K., and Saitoh, N.: Hydroxyl Interannual Variability Impacts Estimation of Regional Methane Emissions, J. Geophys. Res. Atmos., 131, e2025JD044457, https://doi.org/10.1029/2025JD044457, 2026.

Bergamaschi, P., Houweling, S., Segers, A., Krol, M., Frankenberg, C., Scheepmaker, R. A., Dlugokencky, E., Wofsy, S. C., Kort, E. A., Sweeney, C., Schuck, T., Brenninkmeijer, C., Chen, H., Beck, V., and Gerbig, C.: Atmospheric CH_4 in the first decade of the 21st century: Inverse modeling analysis using SCIAMACHY satellite retrievals and NOAA surface measurements, J. Geophys. Res. Atmos., 118, 7350–7369, https://doi.org/10.1002/jgrd.50480, 2013.

Bloom, A. A., Bowman, K. W., Lee, M., Turner, A. J., Schroeder, R., Worden, J. R., Weidner, R., McDonald, K. C., and Jacob, D. J.: A global wetland methane emissions and uncertainty dataset for atmospheric chemical transport models (WetCHARTs version 1.0), Geosci. Model Dev., 10, 2141–2156, https://doi.org/10.5194/gmd-10-2141-2017, 2017.

Botía, S., Gerbig, C., Marshall, J., Lavric, J. V., Walter, D., Pöhlker, C., Holanda, B., Fisch, G., De Araújo, A. C., Sá, M. O., Teixeira, P. R., Resende, A. F., Dias-Junior, C. Q., Van Asperen, H., Oliveira, P. S., Stefanello, M., and Acevedo, O. C.: Understanding nighttime methane signals at the Amazon Tall Tower Observatory (ATTO), Atmos. Chem. Phys., 20, 6583–6606, https://doi.org/10.5194/acp-20-6583-2020, 2020.

Botía, S., Munassar, S., Koch, T., Custodio, D., Basso, L. S., Komiya, S., Lavric, J. V., Walter, D., Gloor, M., Martins, G., Naus, S., Koren, G., Luijkx, I. T., Hantson, S., Miller, J. B., Peters, W., Rödenbeck, C., and Gerbig, C.: Combined CO_2 measurement record indicates Amazon forest carbon uptake is offset by savanna carbon release, Atmos. Chem. Phys., 25, 6219–6255, https://doi.org/10.5194/acp-25-6219-2025, 2025.

Builes-Jaramillo, A., Salas, H. D., Valencia, J., and Florian, C.: Orinoco revisited: Comprehensive analysis of the Orinoco River basin present and future hydroclimate, Atmósfera, 38, https://doi.org/10.20937/ATM.53359, 2024.

Caldana, N. F. D. S., Aguiar E Silva, M. A., Cavatorta, M. G., Ferreira, L. G. B., and Martins, J. A.: Pluviometric variability, water balance and risk of dry spells in the basin of Paraná River III, Brazil, Rev. Geogr., 38, 275, https://doi.org/10.51359/2238-6211.2021.244781, 2021.

Calle, L. and Poulter, B.: Ecosystem age-class dynamics and distribution in the LPJ-wsl v2.0 global ecosystem model, Geosci. Model Dev., 14, 2575–2601, https://doi.org/10.5194/gmd-14-2575-2021, 2021.

Clark, D. B., Mercado, L. M., Sitch, S., Jones, C. D., Gedney, N., Best, M. J., Pryor, M., Rooney, G. G., Essery, R. L. H., Blyth, E., Boucher, O., Harding, R. J., Huntingford, C., and Cox, P. M.: The Joint UK Land Environment Simulator (JULES), model description – Part 2: Carbon fluxes and vegetation dynamics, Geosci. Model Dev., 4, 701–722, https://doi.org/10.5194/gmd-4-701-2011, 2011.

https://doi.org/10.5194/egusphere-2026-5245
Preprint. Discussion started: 28 September 2026

Copernicus Atmosphere Monitoring Service: CAMS global inversion-optimised greenhouse gas fluxes and concentrations, https://doi.org/10.24381/ED2851D2, 2020.

Crippa, M., Guizzardi, D., Solazzo, E., Muntean, M., Schaaf, E., Monforti-Ferrario, F., Banja, M., Olivier, J. G. J., Grassi, G., Rossi, S., and Vignati, E.: GHG emissions of all world countries / European Commission, Joint Research Centre. 2021 report / Crippa, M.; Guizzardi, D.; Solazzo, E.; Muntean, M.; Schaaf, E.; Monforti-Ferrario, F.; Banja, M.; Olivier, J.G.J.; Grassi, G.; Rossi, S.; Vignati, E, https://doi.org/10.2760/173513, 2021.

De Souza Maria, L., Da Costa, L. M., Campos, M. O., Panosso, A. R., Basso, L. S., Da Silva Junior, C. A., and La Scala, N.: Confronting the Amazon’s fire crisis: Evidence of early fire occurrence and increased atmospheric gases from the GOSAT satellite, J. Atmos. Sol.-Terr. Phys., 277, 106652, https://doi.org/10.1016/j.jastp.2025.106652, 2025.

Drumond, A., Marengo, J., Ambrizzi, T., Nieto, R., Moreira, L., and Gimeno, L.: The role of the Amazon Basin moisture in the atmospheric branch of the hydrological cycle: a Lagrangian analysis, Hydrol. Earth Syst. Sci., 18, 2577–2598, https://doi.org/10.5194/hess-18-2577-2014, 2014.

Etiope, G., Ciotoli, G., Schwietzke, S., and Schoell, M.: Gridded maps of geological methane emissions and their isotopic signature, 2019.

Fleischmann, A. S., Papa, F., Fassoni-Andrade, A., Melack, J. M., Wongchuig, S., Paiva, R. C. D., Hamilton, S. K., Fluet-Chouinard, E., Barbedo, R., Aires, F., Al Bitar, A., Bonnet, M.-P., Coe, M., Ferreira-Ferreira, J., Hess, L., Jensen, K., McDonald, K., Ovando, A., Park, E., Parrens, M., Pinel, S., Prigent, C., Resende, A. F., Revel, M., Rosenqvist, A., Rosenqvist, J., Rudorff, C., Silva, T. S. F., Yamazaki, D., and Collischonn, W.: How much inundation occurs in the Amazon River basin?, Remote Sens. Environ., 278, 113099, https://doi.org/10.1016/j.rse.2022.113099, 2022.

Flood, V. A., Strong, K., Whaley, C. H., Walker, K. A., Blumenstock, T., Hannigan, J. W., Mellqvist, J., Notholt, J., Palm, M., Röhling, A. N., Arnold, S., Beagley, S., Chien, R.-Y., Christensen, J., Deushi, M., Dobricic, S., Dong, X., Fu, J. S., Gauss, M., Gong, W., Langner, J., Law, K. S., Marelle, L., Onishi, T., Oshima, N., Plummer, D. A., Pozzoli, L., Raut, J.-C., Thomas, M. A., Tsyro, S., and Turnock, S.: Evaluating modelled tropospheric columns of CH_4 , CO, and O_3 in the Arctic using ground-based Fourier transform infrared (FTIR) measurements, Atmos. Chem. Phys., 24, 1079–1118, https://doi.org/10.5194/acp-24-1079-2024, 2024.

Frappart, F., Papa, F., Malbeteau, Y., León, J., Ramillien, G., Prigent, C., Seoane, L., Seyler, F., and Calmant, S.: Surface Freshwater Storage Variations in the Orinoco Floodplains Using Multi-Satellite Observations, Remote Sens., 7, 89–110, https://doi.org/10.3390/rs70100089, 2014.

Gatti, L. V., Correa, C. C. S., Domingues, L. G., Miller, J. B., Gloor, M., Martinewski, A., Basso, L. S., Santana, R., Crispim, S. P., Marani, L., and Neves, R. L.: CH4 Aircraft Vertical

https://doi.org/10.5194/egusphere-2026-5245
Preprint. Discussion started: 28 September 2026

Profiles Measurements at Four Amazonian Sites Between 2010 and 2018, , https://doi.org/10.1594/PANGAEA.934596, 2021.

Gloor, M., Gatti, L. V., Wilson, C., Parker, R. J., Boesch, H., Popa, E., Chipperfield, M. P., Poulter, B., Zhang, Z., Basso, L., Miller, J., McNorton, J., Jimenez, C., and Prigent, C.: Large Methane Emissions From the Pantanal During Rising Water-Levels Revealed by Regularly Measured Lower Troposphere CH_4 Profiles, Glob. Biogeochem. Cycles, 35, e2021GB006964, https://doi.org/10.1029/2021GB006964, 2021.

Ham, J. van (Ed.): Non-CO_2 greenhouse gases: scientific understanding, control, and implementationProceedings of the Second International Symposium, Noordwijkerhout, the Netherlands, 8-10 September 1999, Springer-Science+Business Media, B. V, Dordrecht, [Netherlands], 1 pp., 2000.

Hancock, S. E., Jacob, D. J., Chen, Z., Nesser, H., Davitt, A., Varon, D. J., Sulprizio, M. P., Balasus, N., Estrada, L. A., Cazorla, M., Dawidowski, L., Diez, S., East, J. D., Penn, E., Randles, C. A., Worden, J., Aben, I., Parker, R. J., and Maasakkers, J. D.: Satellite quantification of methane emissions from South American countries: a high-resolution inversion of TROPOMI and GOSAT observations, Atmos. Chem. Phys., 25, 797–817, https://doi.org/10.5194/acp-25-797-2025, 2025a.

Hancock, S. E., Jacob, D. J., Chen, Z., Nesser, H., Davitt, A., Varon, D. J., Sulprizio, M. P., Balasus, N., Estrada, L. A., Cazorla, M., Dawidowski, L., Diez, S., East, J. D., Penn, E., Randles, C. A., Worden, J., Aben, I., Parker, R. J., and Maasakkers, J. D.: Satellite quantification of methane emissions from South American countries: a high-resolution inversion of TROPOMI and GOSAT observations, Atmos. Chem. Phys., 25, 797–817, https://doi.org/10.5194/acp-25-797-2025, 2025b.

Heimann, M. and K¨orner, S.: The Global Atmospheric Tracer Model TM3, n.d.

Hess, L. L., Melack, J. M., Affonso, A. G., Barbosa, C., Gastil-Buhl, M., and Novo, E. M. L. M.: Wetlands of the Lowland Amazon Basin: Extent, Vegetative Cover, and Dual-season Inundated Area as Mapped with JERS-1 Synthetic Aperture Radar, Wetlands, 35, 745–756, https://doi.org/10.1007/s13157-015-0666-y, 2015.

Hossaini, R., Chipperfield, M. P., Saiz-Lopez, A., Fernandez, R., Monks, S., Feng, W., Brauer, P., and Von Glasow, R.: A global model of tropospheric chlorine chemistry: Organic versus inorganic sources and impact on methane oxidation, J. Geophys. Res. Atmos., 121, https://doi.org/10.1002/2016JD025756, 2016.

Huijnen, V., Williams, J., Van Weele, M., Van Noije, T., Krol, M., Dentener, F., Segers, A., Houweling, S., Peters, W., De Laat, J., Boersma, F., Bergamaschi, P., Van Velthoven, P., Le Sager, P., Eskes, H., Alkemade, F., Scheele, R., Nédélec, P., and Pätz, H.-W.: The global chemistry transport model TM5: description and evaluation of the tropospheric chemistry version 3.0, Geosci. Model Dev., 3, 445–473, https://doi.org/10.5194/gmd-3-445-2010, 2010.

Huntzinger, D. N., SCHWALM, C. R., WEI, `Y, COOK, R. B., and MICHALAK, A. M.: NACP MsTMIP: Global 0.5-degree Model Outputs in Standard Format, Version 1.0, https://doi.org/10.3334/ORNLDAAC/1225, 2026.

ICOS RI, Bergamaschi, P., Colomb, A., De Mazière, M., Emmenegger, L., Kubistin, D., Lehner, I., Lehtinen, K., Lund Myhre, C., Marek, M., O'Doherty, S., Platt, S. M., Plaß-Dülmer, C., Ramonet, M., Apadula, F., Arnold, S., Blanc, P.-E., Brunner, D., Chen, H., Chmura, L., Conil, S., Couret, C., Cristofanelli, P., Delmotte, M., Forster, G., Frumau, A., Gheusi, F., Hammer, S., Haszpra, L., Hatakka, J., Heliasz, M., Henne, S., Hoheisel, A., Kneuer, T., Laurila, T., Leskinen, A., Leuenberger, M., Levin, I., Lindauer, M., Lunder, C., Mammarella, I., Manca, G., Manning, A., Martin, D., Meinhardt, F., Mölder, M., Müller-Williams, J., Necki, J., Ottosson-Löfvenius, M., Philippon, C., Piacentino, S., Pitt, J., Rivas-Soriano, P., Scheeren, B., Schumacher, M., Sha, M. K., Smith, P., Spain, G., Steinbacher, M., Sørensen, L. L., Vermeulen, A., Vítková, G., Xueref-Remy, I., di Sarra, A., Conen, F., Kazan, V., Roulet, Y.-A., Biermann, T., Heltai, D., Hensen, A., Hermansen, O., Komínková, K., Laurent, O., Levula, J., Lopez, M., Marklund, P., Pichon, J.-M., Schmidt, M., Stanley, K., Trisolino, P., ICOS Carbon Portal, ICOS Atmosphere Thematic Centre, ICOS Flask And Calibration Laboratory, and ICOS Central Radiocarbon Laboratory: European Obspack compilation of atmospheric methane data from ICOS and non-ICOS European stations for the period 1984-2024; obspack_ch4_466_GVeu_2024-02-01 (1.0), https://doi.org/10.18160/KDMT-V6CG, 2024.

Jackson, R. B., Saunois, M., Bousquet, P., Canadell, J. G., Poulter, B., Stavert, A. R., Bergamaschi, P., Niwa, Y., Segers, A., and Tsuruta, A.: Increasing anthropogenic methane emissions arise equally from agricultural and fossil fuel sources, Environ. Res. Lett., 15, 071002, https://doi.org/10.1088/1748-9326/ab9ed2, 2020.

Janardanan, R., Maksyutov, S., Tsuruta, A., Wang, F., Tiwari, Y. K., Valsala, V., Ito, A., Yoshida, Y., Kaiser, J. W., Janssens-Maenhout, G., Arshinov, M., Sasakawa, M., Tohjima, Y., Worthy, D. E. J., Dlugokencky, E. J., Ramonet, M., Arduini, J., Lavric, J. V., Piacentino, S., Krummel, P. B., Langenfelds, R. L., Mammarella, I., and Matsunaga, T.: Country-Scale Analysis of Methane Emissions with a High-Resolution Inverse Model Using GOSAT and Surface Observations, Remote Sens., 12, 375, https://doi.org/10.3390/rs12030375, 2020.

Jockel, P., Tost, H., Pozzer, A., Sander, R., Steil, B., Stiller, G., Tanarhte, M., Taraborrelli, D., van Aardenne, J., and Lelieveld, J.: The atmospheric chemistry general circulation model ECHAM5/MESSy1: consistent simulation of ozone from the surface to the mesosphere, Atmos Chem Phys, 2006.

Kalnay, E., Kanamitsu, M., Kistler, R., Collins, W., Deaven, D., Gandin, L., Iredell, M., Saha, S., White, G., Woollen, J., Zhu, Y., Leetmaa, A., Reynolds, R., Chelliah, M., Ebisuzaki, W., Higgins, W., Janowiak, J., Mo, K. C., Ropelewski, C., Wang, J., Jenne, R., and Joseph, D.: The NCEP/NCAR 40-Year Reanalysis Project, Bull. Am. Meteorol. Soc., 77, 437–471, https://doi.org/10.1175/1520-0477(1996)077%3C0437:TNYRP%3E2.0.CO;2, 1996.

Kirschke, S., Bousquet, P., Ciais, P., Saunois, M., Canadell, J. G., Dlugokencky, E. J., Bergamaschi, P., Bergmann, D., Blake, D. R., Bruhwiler, L., Cameron-Smith, P., Castaldi, S., Chevallier, F., Feng, L., Fraser, A., Heimann, M., Hodson, E. L., Houweling, S., Josse, B.,

https://doi.org/10.5194/egusphere-2026-5245
Preprint. Discussion started: 28 September 2026

Fraser, P. J., Krummel, P. B., Lamarque, J.-F., Langenfelds, R. L., Le Quéré, C., Naik, V., O'Doherty, S., Palmer, P. I., Pison, I., Plummer, D., Poulter, B., Prinn, R. G., Rigby, M., Ringeval, B., Santini, M., Schmidt, M., Shindell, D. T., Simpson, I. J., Spahni, R., Steele, L. P., Strode, S. A., Sudo, K., Szopa, S., Van Der Werf, G. R., Voulgarakis, A., Van Weele, M., Weiss, R. F., Williams, J. E., and Zeng, G.: Three decades of global methane sources and sinks, Nat. Geosci., 6, 813–823, https://doi.org/10.1038/ngeo1955, 2013.

Kleinen, T., Mikolajewicz, U., and Brovkin, V.: Terrestrial methane emissions from the Last Glacial Maximum to the preindustrial period, Clim. Past, 16, 575–595, https://doi.org/10.5194/cp-16-575-2020, 2020.

Lehner, B. and Döll, P.: Development and validation of a global database of lakes, reservoirs and wetlands, J. Hydrol., 296, 1–22, https://doi.org/10.1016/j.jhydrol.2004.03.028, 2004.

Lehner, B. and Grill, G.: Global river hydrography and network routing: baseline data and new approaches to study the world's large river systems, Hydrol. Process., 27, 2171–2186, https://doi.org/10.1002/hyp.9740, 2013.

Liu, L., Zhuang, Q., Oh, Y., Shurpali, N. J., Kim, S., and Poulter, B.: Uncertainty Quantification of Global Net Methane Emissions From Terrestrial Ecosystems Using a Mechanistically Based Biogeochemistry Model, J. Geophys. Res. Biogeosciences, 125, e2019JG005428, https://doi.org/10.1029/2019JG005428, 2020.

Melack, J. M., Hess, L. L., Gastil, M., Forsberg, B. R., Hamilton, S. K., Lima, I. B. T., and Novo, E. M. L. M.: Regionalization of methane emissions in the Amazon Basin with microwave remote sensing, Glob. Change Biol., 10, 530–544, https://doi.org/10.1111/j.1365-2486.2004.00763.x, 2004.

Melack, J. M., Basso, L. S., Fleischmann, A. S., Botía, S., Guo, M., Zhou, W., Barbosa, P. M., Amaral, J. H. F., and MacIntyre, S.: Challenges Regionalizing Methane Emissions Using Aquatic Environments in the Amazon Basin as Examples, Front. Environ. Sci., 10, 866082, https://doi.org/10.3389/fenvs.2022.866082, 2022.

Miller, J. B., Gatti, L. V., d'Amelio, M. T. S., Crotwell, A. M., Dlugokencky, E. J., Bakwin, P., Artaxo, P., and Tans, P. P.: Airborne measurements indicate large methane emissions from the eastern Amazon basin, Geophys. Res. Lett., 34, 2006GL029213, https://doi.org/10.1029/2006GL029213, 2007.

Miller, J. B., Giordane A. Martins, De Souza, R. A. F., and Schuldt, K. N.: Manaus aircraft profile data for the period 2017-2023; obspack_multi-species_1_manaus_profiles_v2.0_2023-09-26, https://doi.org/10.25925/20230922, 2023.

Monks, S. A., Arnold, S. R., Hollaway, M. J., Pope, R. J., Wilson, C., Feng, W., Emmerson, K. M., Kerridge, B. J., Latter, B. L., Miles, G. M., Siddans, R., and Chipperfield, M. P.: The TOMCAT global chemical transport model v1.6: description of chemical mechanism and

https://doi.org/10.5194/egusphere-2026-5245
Preprint. Discussion started: 28 September 2026

model evaluation, Geosci. Model Dev., 10, 3025–3057, https://doi.org/10.5194/gmd-10-3025-2017, 2017.

Nascimento, S. C. D., Melo, M. M. M., and Paz, A. R. D.: River-floodplain interaction and flood wave routing along rivers flowing through Pantanal wetlands, J. South Am. Earth Sci., 125, 104296, https://doi.org/10.1016/j.jsames.2023.104296, 2023.

Neves, R. A. L., Gatti, L. V., Cunha, C. L., Correia, C. S. C., Silva, F. M., Machado, G. B. M., Morais, C. S., Lopes, F. L., Domingues, L. G., Sanches, A. H., Arai, E., Malacarne, M., Guerra, J. C., and Marani, L.: The impact of reduced precipitation on methane emissions in the Amazon and its role in the global methane balance, Atmos. Environ., 372, 121860, https://doi.org/10.1016/j.atmosenv.2026.121860, 2026.

Nisbet, E. G.: Climate feedback on methane from wetlands, Nat. Clim. Change, 13, 421–422, https://doi.org/10.1038/s41558-023-01634-3, 2023.

Nisbet, E. G., Dlugokencky, E. J., Manning, M. R., Lowry, D., Fisher, R. E., France, J. L., Michel, S. E., Miller, J. B., White, J. W. C., Vaughn, B., Bousquet, P., Pyle, J. A., Warwick, N. J., Cain, M., Brownlow, R., Zazzeri, G., Lanoisellé, M., Manning, A. C., Gloor, E., Worthy, D. E. J., Brunke, E. -G., Labuschagne, C., Wolff, E. W., and Ganesan, A. L.: Rising atmospheric methane: 2007–2014 growth and isotopic shift, Glob. Biogeochem. Cycles, 30, 1356–1370, https://doi.org/10.1002/2016GB005406, 2016.

Nisbet, E. G., Manning, M. R., Dlugokencky, E. J., Fisher, R. E., Lowry, D., Michel, S. E., Myhre, C. L., Platt, S. M., Allen, G., Bousquet, P., Brownlow, R., Cain, M., France, J. L., Hermansen, O., Hossaini, R., Jones, A. E., Levin, I., Manning, A. C., Myhre, G., Pyle, J. A., Vaughn, B. H., Warwick, N. J., and White, J. W. C.: Very Strong Atmospheric Methane Growth in the 4 Years 2014–2017: Implications for the Paris Agreement, Glob. Biogeochem. Cycles, 33, 318–342, https://doi.org/10.1029/2018GB006009, 2019.

Oh, Y., Bruhwiler, L., Lan, X., Basu, S., Schuldt, K., Thoning, K., Michel, S. E., Clark, R., Miller, J. B., Andrews, A., Sherwood, O., Etiope, G., Crippa, M., Liu, L., Zhuang, Q., Randerson, J., van der Werf, G., Aalto, T., Amendola, S., Andra, S. C., Andrade, M., Nguyen, N. A., Aoki, S., Apadula, F., Arifin, I. B., Arnold, S., Arshinov, M., Baier, B., Bergamaschi, P., Biermann, T., Biraud, S. C., Blanc, P.-E., Brailsford, G., Chen, H., Colomb, A., Couret, C., Cristofanelli, P., Cuevas, E., Chmura, L., Delmotte, M., Emmenegger, L., Esenzhanova, G., Fujita, R., Gatti, L., Guerette, E.-A., Haszpra, L., Heliasz, M., Hermansen, O., Holst, J., Di lorio, T., Jordan, A., Jennifer, M.-W., Karion, A., Kawasaki, T., Kazan, V., Keronen, P., Kim, S.-Y., Kneuer, T., Kominkova, K., Kozlova, E., Krummel, P., Kubistin, D., Labuschagne, C., Langenfelds, R., Laurent, O., Laurila, T., Lee, H., Lehner, I., Leuenberger, M., Lindauer, M., Lopez, M., Mahdi, R., Mammarella, I., Manca, G., Marek, M. V., Mazière, M. D., McKain, K., Meinhardt, F., Miller, C. E., Mölder, M., Moncrieff, J., Moosen, H., Moreno, C., Morimoto, S., Myhre, C. L., Nahas, A. C., Necki, J., Nichol, S., O'Doherty, S., Paramonova, N., Piacentino, S., Pichon, J. M., Plass-Dülmer, C., Ramonet, M., Ries, L., di Sarra, A. G., Sasakawa, M., Say, D., Schaefer, H., et al.: CarbonTracker CH4 2023, https://doi.org/10.25925/40JT-QD67, 2023.

Oh, Y., Bruhwiler, L., Lan, X., Halder, S., Riddell-Young, B., Basu, S., Miller, J. B., Michel, S., Schuldt, K., Andrews, A., Biraud, S., Chmura, Ł., Lorio, T. D., Guerette, E.-A., Kozlova, E., Liu, L., Montaguti, S., Morimoto, S., Steinbacher, M., Umezawa, T., Xueref-Remy, I., and Zazzeri, G.: Isotopic constraints in methane inversions reveal larger trends in wetland emissions with improved linkage to terrestrial water storage, Nat. Commun., https://doi.org/10.1038/s41467-026-74777-4, 2026.

Pangala, S. R., Enrich-Prast, A., Basso, L. S., Peixoto, R. B., Bastviken, D., Hornibrook, E. R. C., Gatti, L. V., Marotta, H., Calazans, L. S. B., Sakuragui, C. M., Bastos, W. R., Malm, O., Gloor, E., Miller, J. B., and Gauci, V.: Large emissions from floodplain trees close the Amazon methane budget, Nature, 552, 230–234, https://doi.org/10.1038/nature24639, 2017.

Parker, R. J., Boesch, H., McNorton, J., Comyn-Platt, E., Gloor, M., Wilson, C., Chipperfield, M. P., Hayman, G. D., and Bloom, A. A.: Evaluating year-to-year anomalies in tropical wetland methane emissions using satellite CH4 observations, Remote Sens. Environ., 211, 261–275, https://doi.org/10.1016/j.rse.2018.02.011, 2018.

Parker, R. J., Webb, A., Boesch, H., Somkuti, P., Barrio Guillo, R., Di Noia, A., Kalaitzi, N., Anand, J. S., Bergamaschi, P., Chevallier, F., Palmer, P. I., Feng, L., Deutscher, N. M., Feist, D. G., Griffith, D. W. T., Hase, F., Kivi, R., Morino, I., Notholt, J., Oh, Y.-S., Ohyama, H., Petri, C., Pollard, D. F., Roehl, C., Sha, M. K., Shiomi, K., Strong, K., Sussmann, R., Té, Y., Velazco, V. A., Warneke, T., Wennberg, P. O., and Wunch, D.: A decade of GOSAT Proxy satellite CH_4 observations, Earth Syst. Sci. Data, 12, 3383–3412, https://doi.org/10.5194/essd-12-3383-2020, 2020.

Patra, P. K., Houweling, S., Krol, M., Bousquet, P., Belikov, D., Bergmann, D., Bian, H., Cameron-Smith, P., Chipperfield, M. P., Corbin, K., Fortems-Cheiney, A., Fraser, A., Gloor, E., Hess, P., Ito, A., Kawa, S. R., Law, R. M., Loh, Z., Maksyutov, S., Meng, L., Palmer, P. I., Prinn, R. G., Rigby, M., Saito, R., and Wilson, C.: TransCom model simulations of CH_4 and related species: linking transport, surface flux and chemical loss with CH_4 variability in the troposphere and lower stratosphere, Atmos. Chem. Phys., 11, 12813–12837, https://doi.org/10.5194/acp-11-12813-2011, 2011.

Ribeiro, I. O., Andreoli, R. V., Kayano, M. T., De Sousa, T. R., Medeiros, A. S., Guimarães, P. C., Barbosa, C. G. G., Godoi, R. H. M., Martin, S. T., and De Souza, R. A. F.: Impact of the biomass burning on methane variability during dry years in the Amazon measured from an aircraft and the AIRS sensor, Sci. Total Environ., 624, 509–516, https://doi.org/10.1016/j.scitotenv.2017.12.147, 2018.

Rigby, M., Montzka, S. A., Prinn, R. G., White, J. W. C., Young, D., O'Doherty, S., Lunt, M. F., Ganesan, A. L., Manning, A. J., Simmonds, P. G., Salameh, P. K., Harth, C. M., Mühle, J., Weiss, R. F., Fraser, P. J., Steele, L. P., Krummel, P. B., McCulloch, A., and Park, S.: Role of atmospheric oxidation in recent methane growth, Proc. Natl. Acad. Sci., 114, 5373–5377, https://doi.org/10.1073/pnas.1616426114, 2017.

https://doi.org/10.5194/egusphere-2026-5245
Preprint. Discussion started: 28 September 2026

Rödenbeck, C.: Estimating CO2 sources and sinks from atmo- spheric mixing ratio measurements using a global inversion of atmospheric transport, Tech. rep., Max Planck Institute for Biogeochemistry, 2005.

Saunois, M., Bousquet, P., Poulter, B., Peregon, A., Ciais, P., Canadell, J. G., Dlugokencky, E. J., Etiope, G., Bastviken, D., Houweling, S., Janssens-Maenhout, G., Tubiello, F. N., Castaldi, S., Jackson, R. B., Alexe, M., Arora, V. K., Beerling, D. J., Bergamaschi, P., Blake, D. R., Brailsford, G., Bruhwiler, L., Crevoisier, C., Crill, P., Covey, K., Frankenberg, C., Gedney, N., Höglund-Isaksson, L., Ishizawa, M., Ito, A., Joos, F., Kim, H.-S., Kleinen, T., Krummel, P., Lamarque, J.-F., Langenfelds, R., Locatelli, R., Machida, T., Maksyutov, S., Melton, J. R., Morino, I., Naik, V., O'Doherty, S., Parmentier, F.-J. W., Patra, P. K., Peng, C., Peng, S., Peters, G. P., Pison, I., Prinn, R., Ramonet, M., Riley, W. J., Saito, M., Santini, M., Schroeder, R., Simpson, I. J., Spahni, R., Takizawa, A., Thornton, B. F., Tian, H., Tohjima, Y., Viovy, N., Voulgarakis, A., Weiss, R., Wilton, D. J., Wiltshire, A., Worthy, D., Wunch, D., Xu, X., Yoshida, Y., Zhang, B., Zhang, Z., and Zhu, Q.: Variability and quasi-decadal changes in the methane budget over the period 2000–2012, Atmos. Chem. Phys., 17, 11135–11161, https://doi.org/10.5194/acp-17-11135-2017, 2017.

Saunois, M., Martinez, A., Poulter, B., Zhang, Z., Raymond, P., Regnier, P., Canadell, J. G., Jackson, R. B., Patra, P. K., Bousquet, P., Ciais, P., Dlugokencky, E. J., Lan, X., Allen, G. H., Bastviken, D., Beerling, D. J., Belikov, D. A., Blake, D. R., Castaldi, S., Crippa, M., Deemer, B. R., Dennison, F., Etiope, G., Gedney, N., Höglund-Isaksson, L., Holgerson, M. A., Hopcroft, P. O., Hugelius, G., Ito, A., Jain, A. K., Janardanan, R., Johnson, M. S., Kleinen, T., Krummel, P., Lauerwald, R., Li, T., Liu, X., McDonald, K. C., Melton, J. R., Mühle, J., Müller, J., Murguia-Flores, F., Niwa, Y., Noce, S., Pan, S., Parker, R. J., Peng, C., Ramonet, M., Riley, W. J., Rocher-Ros, G., Rosentreter, J. A., Sasakawa, M., Segers, A., Smith, S. J., Stanley, E. H., Thanwerdas, J., Tian, H., Tsuruta, A., Tubiello, F. N., Weber, T. S., Van Der Werf, G., Worthy, D. E., Xi, Y., Yoshida, Y., Zhang, W., Zheng, B., Zhu, Q., Zhu, Q., and Zhuang, Q.: Global Methane Budget 2000–2020, https://doi.org/10.5194/essd-2024-115, 6 June 2024.

Saunois, M., Martinez, A., Poulter, B., Zhang, Z., Raymond, P. A., Regnier, P., Canadell, J. G., Jackson, R. B., Patra, P. K., Bousquet, P., Ciais, P., Dlugokencky, E. J., Lan, X., Allen, G. H., Bastviken, D., Beerling, D. J., Belikov, D. A., Blake, D. R., Castaldi, S., Crippa, M., Deemer, B. R., Dennison, F., Etiope, G., Gedney, N., Höglund-Isaksson, L., Holgerson, M. A., Hopcroft, P. O., Hugelius, G., Ito, A., Jain, A. K., Janardanan, R., Johnson, M. S., Kleinen, T., Krummel, P. B., Lauerwald, R., Li, T., Liu, X., McDonald, K. C., Melton, J. R., Mühle, J., Müller, J., Murguia-Flores, F., Niwa, Y., Noce, S., Pan, S., Parker, R. J., Peng, C., Ramonet, M., Riley, W. J., Rocher-Ros, G., Rosentreter, J. A., Sasakawa, M., Segers, A., Smith, S. J., Stanley, E. H., Thanwerdas, J., Tian, H., Tsuruta, A., Tubiello, F. N., Weber, T. S., Van Der Werf, G. R., Worthy, D. E. J., Xi, Y., Yoshida, Y., Zhang, W., Zheng, B., Zhu, Q., Zhu, Q., and Zhuang, Q.: Global Methane Budget 2000–2020, Earth Syst. Sci. Data, 17, 1873–1958, https://doi.org/10.5194/essd-17-1873-2025, 2025.

Schuldt, K. N., Mund, J., Aalto, T., Aaltonen, H., Abshire, J. B., Aikin, K., Allen, G., Andrade, M., Apadula, F., Arnold, S., Baier, B., Bakwin, P., Bäni, L., Bartyzel, J., Bentz, G., Bergamaschi, P., Beyersdorf, A., Biermann, T., Biraud, S. C., Pierre-Eric Blanc, Boenisch, H., Bowling, D., Brailsford, G., Brand, W. A., Brunner, D., Bui, T. P. V., van den Bulk, P., Benoit

Burban, Francescopiero Calzolari, Chang, C. S., Chen, G., Huilin Chen, Lukasz Chmura, St. Clair, J. M., Clark, S., Sites Climadat, Coletta, J. D., Colomb, A., Commane, R., Condori, L., Conen, F., Conil, S., Couret, C., Cristofanelli, P., Cuevas, E., Curcoll, R., Daube, B., Davis, K. J., Dean-Day, J. M., Delmotte, M., Dickerson, R., DiGangi, E., DiGangi, J. P., Elsasser, M., Emmenegger, L., Shuangxi Fang, Forster, G., France, J., Frumau, A., Fuente-Lastra, M., Galkowski, M., Gatti, L. V., Gehrlein, T., Gerbig, C., Francois Gheusi, Gloor, E., Goto, D., Griffis, T., Hammer, S., Hanisco, T. F., Hanson, C., Hashimoto, S., Haszpra, L., Hatakka, J., Heimann, M., Heliasz, M., Heltai, D., Henne, S., Hensen, A., Hermans, C., Hermansen, O., Higgs, J., Hintsa, E., Hoheisel, A., Holst, J., Di Iorio, T., Iraci, L. T., Ivakhov, V., Jaffe, D. A., Joly, L., Jordan, A., Joubert, W., Kang, H.-Y., Karion, A., Kawa, S. R., Kazan, V., Keeling, R. F., Ishijima Kentaro, Keronen, P., et al.: Multi-laboratory compilation of atmospheric carbon dioxide data for the period 1957-2024; obspack_co2_1_GLOBALVIEWplus_v11.0_2026-01-12, https://doi.org/10.25925/20250801, 2025.

Schwietzke, S., Sherwood, O. A., Bruhwiler, L. M. P., Miller, J. B., Etiope, G., Dlugokencky, E. J., Michel, S. E., Arling, V. A., Vaughn, B. H., White, J. W. C., and Tans, P. P.: Upward revision of global fossil fuel methane emissions based on isotope database, Nature, 538, 88–91, https://doi.org/10.1038/nature19797, 2016.

Segers, N.: Contribution to documentation of products and services as provided within the scope of this contract – 2023 – Part CH4, 2023.

Spahni, R., Wania, R., Neef, L., Van Weele, M., Pison, I., Bousquet, P., Frankenberg, C., Foster, P. N., Joos, F., Prentice, I. C., and Van Velthoven, P.: Constraining global methane emissions and uptake by ecosystems, Biogeosciences, 8, 1643–1665, https://doi.org/10.5194/bg-8-1643-2011, 2011.

Spivakovsky, C. M., Logan, J. A., Montzka, S. A., Balkanski, Y. J., Foreman-Fowler, M., Jones, D. B. A., Horowitz, L. W., Fusco, A. C., Brenninkmeijer, C. A. M., Prather, M. J., Wofsy, S. C., and McElroy, M. B.: Three-dimensional climatological distribution of tropospheric OH: Update and evaluation, J. Geophys. Res. Atmos., 105, 8931–8980, https://doi.org/10.1029/1999JD901006, 2000.

Thoning, K., Dlugokencky, E., Lan, X., and NOAA Global Monitoring Laboratory: Trends in globally-averaged CH4, N2O, and SF6, https://doi.org/10.15138/P8XG-AA10, 2022.

Tunnicliffe, R. L., Ganesan, A. L., Parker, R. J., Boesch, H., Gedney, N., Poulter, B., Zhang, Z., Lavrič, J. V., Walter, D., Rigby, M., Henne, S., Young, D., and O'Doherty, S.: Quantifying sources of Brazil's CH_4 emissions between 2010 and 2018 from satellite data, Atmos. Chem. Phys., 20, 13041–13067, https://doi.org/10.5194/acp-20-13041-2020, 2020.

Turner, A. J., Frankenberg, C., Wennberg, P. O., and Jacob, D. J.: Ambiguity in the causes for decadal trends in atmospheric methane and hydroxyl, Proc. Natl. Acad. Sci., 114, 5367–5372, https://doi.org/10.1073/pnas.1616020114, 2017.

https://doi.org/10.5194/egusphere-2026-5245
Preprint. Discussion started: 28 September 2026

Turner, A. J., Frankenberg, C., and Kort, E. A.: Interpreting contemporary trends in atmospheric methane, Proc. Natl. Acad. Sci., 116, 2805–2813, https://doi.org/10.1073/pnas.1814297116, 2019.

Van Asperen, H., Alves-Oliveira, J. R., Warneke, T., Forsberg, B., De Araújo, A. C., and Notholt, J.: The role of termite CH_4 emissions on the ecosystem scale: a case study in the Amazon rainforest, Biogeosciences, 18, 2609–2625, https://doi.org/10.5194/bg-18-2609-2021, 2021.

Van Asperen, H., Komiya, S., Jones, S., Botia, S., Lavric, J., Warneke, T., Griffith, D., and Trumbore, S.: Unique Tall Tower Greenhouse Gas Measurements in the Amazon Rainforest: observed patterns and daily cycles, , https://doi.org/10.5194/egusphere-egu23-10522, 2023.

Wang, M. and Fu, Q.: Stratosphere-Troposphere Exchange of Air Masses and Ozone Concentrations Based on Reanalyses and Observations, J. Geophys. Res. Atmos., 126, e2021JD035159, https://doi.org/10.1029/2021JD035159, 2021.

Weber, T., Wiseman, N. A., and Kock, A.: Global ocean methane emissions dominated by shallow coastal waters, Nat. Commun., 10, 4584, https://doi.org/10.1038/s41467-019-12541-7, 2019.

Wilson, C., Gloor, M., Gatti, L. V., Miller, J. B., Monks, S. A., McNorton, J., Bloom, A. A., Basso, L. S., and Chipperfield, M. P.: Contribution of regional sources to atmospheric methane over the Amazon Basin in 2010 and 2011, Glob. Biogeochem. Cycles, 30, 400–420, https://doi.org/10.1002/2015GB005300, 2016.

Wilson, C., Chipperfield, M. P., Gloor, M., Parker, R. J., Boesch, H., McNorton, J., Gatti, L. V., Miller, J. B., Basso, L. S., and Monks, S. A.: Large and increasing methane emissions from eastern Amazonia derived from satellite data, 2010–2018, Atmos. Chem. Phys., 21, 10643–10669, https://doi.org/10.5194/acp-21-10643-2021, 2021.

Zhang, Z., Poulter, B., Feldman, A. F., Ying, Q., Ciais, P., Peng, S., and Li, X.: Recent intensification of wetland methane feedback, Nat. Clim. Change, 13, 430–433, https://doi.org/10.1038/s41558-023-01629-0, 2023.

Zhao, Y., Saunois, M., Bousquet, P., Lin, X., Berchet, A., Hegglin, M. I., Canadell, J. G., Jackson, R. B., Dlugokencky, E. J., Langenfelds, R. L., Ramonet, M., Worthy, D., and Zheng, B.: Influences of hydroxyl radicals (OH) on top-down estimates of the global and regional methane budgets, Atmos. Chem. Phys., 20, 9525–9546, https://doi.org/10.5194/acp-20-9525-2020, 2020.

Zhou, M., Langerock, B., Vigouroux, C., Sha, M. K., Ramonet, M., Delmotte, M., Mahieu, E., Bader, W., Hermans, C., Kumps, N., Metzger, J.-M., Duflot, V., Wang, Z., Palm, M., and De Mazière, M.: Atmospheric CO and CH_4 time series and seasonal variations on Reunion Island from ground-based in situ and FTIR (NDACC and TCCON) measurements, Atmos. Chem. Phys., 18, 13881–13901, https://doi.org/10.5194/acp-18-13881-2018, 2018.

https://doi.org/10.5194/egusphere-2026-5245
Preprint. Discussion started: 28 September 2026

Zhuang, Q., Chen, M., Xu, K., Tang, J., Saikawa, E., Lu, Y., Melillo, J. M., Prinn, R. G., and McGuire, A. D.: Response of global soil consumption of atmospheric methane to changes in atmospheric climate and nitrogen deposition, Glob. Biogeochem. Cycles, 27, 650–663, https://doi.org/10.1002/gbc.20057, 2013.